University of Alberta

Natural zeolite membranes for gas and liquid separations

By

Paul D. Swenson

A thesis submitted to the Faculty of Graduate Studies and Research

in partial fulfillment of the requirements for the degree of

Master of Science

in

Chemical Engineering

Department of Chemical and Materials Engineering

Fall 2012

Edmonton, Alberta

Abstract

Synthetic zeolitic membranes have received much research attention over the past several decades but few studies have examined the potential application of natural zeolites for membrane separations. In this study two separate high density natural zeolite deposits were identified, characterized and experiments were performed separating gases and liquids using these robust membranes.

As-mined, raw clinoptilolite membranes showed industrially relevant permeances and selectivities of hydrogen over carbon dioxide and light hydrocarbons above Knudsen selectivity. This is indicative of activated diffusion through zeolitic pores. A simple alkaline membrane pre-treatment increases thermal stability and further increases hydrogen selectivity to well above Knudsen selectivity.

Desalination of a synthetic seawater and purification of a synthetic process water was also performed. High ion rejection and efficient fluxes were found for pervaporative desalination experiments. The synthetic process water showed similar results while also exhibiting high rejection to a model organic compound.

Further investigations are required before industrial application can be considered but these studies clearly indicate that natural zeolite membranes are not only feasible but show great potential as alternatives to their synthetic analogs.

Acknowledgments

I wouldn't be where I am today and I wouldn't be who I am today if I hadn't disrupted Dr. S. M. Kuznicki's thermodynamics lecture 5 years ago, abruptly inquiring if he would hire me as an undergraduate student in his laboratories. Over the past 5 years he has given me boundless technical and creative freedom and has become my supervisor, my colleague, my friend and without a doubt in my mind the best mentor a young professional could ask for.

W. An has become a Mother to me; encouraging and congratulating my achievements while always steering me back in the right direction.

B. Tanchuk for always making time for a coffee or something stronger. Your support has been integral to my academic and personal life.

A. Gupta, A. Warnock, and E. Bastida and everyone in the lab for giving me support inside and outside the lab.

A. Zeko and Dr. A. Drambrowitz for taking the extra time to help improve my technical writing abilities.

My family has always shown unconditional love and support. The love they have given me cannot be expressed in words.

My friends, A. Parrish, M. Shewchuk, E. Elton, A. Mclaughlin and everyone else, for always having a caring supportive ear for me to pour my thoughts into.

Table of Contents

List of Figures

List of Tables

Nomenclature

A	Effective Membrane Area
Å	Angstrom
BET	Brunauer, Emmett and Teller
BTU	British Thermal Unit
^{o}C	Degrees Celsius
cc	Cubic Centimetre
cm	Centimeter
cm^3	Cubic Centimeter
EDX	Energy Dispersive X-Ray Spectroscopy
F	Flux
g	grams
GC-FID	Gas Chromatography with a Flame Ionization Detector
h	Hour
HEU	International Zeolite Association Framework Type Code
i	Component i
in.	Inches
ICDD-PDF	International Center for Diffraction Data-Powder Diffraction File
IZA	International Zeolite Association

j	Component j
kg	Kilogram
km^3	Square Kilometers
kPa	KiloPascal
kV	Kilovolt
L	Litre
M	Molar Mass
m^2	Square Meters
m^3	Cubic Meters
MPa	MegaPascal
µm	Micrometer
min	Minute
mL	Millilitre
mm	Millimeter
mol	Moles
N	Molar Flux
NES	Not Enough Sample
P	Permeance
p	Partial Pressure

Pa	Pascals
PSA	Pressure Swing Adsorption
S	Selectivity
s	Seconds
SAGD	Steam Assisted Gravity Drainage
SEM	Scanning Electron Microscopy
SOR	Steam to Oil Ratio
STP	Standard Temperature and Pressure
t	Run Length
W	Weight
wt%	Weight Percent
XRD	X-Ray Diffraction

Chapter 1. Introduction

1.0 Overview

Significant membrane technology research and development effort has been focused on investigating new membrane materials. Ideally, membrane materials should combine high thermal and chemical stability with mechanical strength. Synthetic zeolites membranes have a uniformly porous structure, which would be ideal for separations, but, unfortunately, synthetic zeolites lack the robustness required for industrial applications.

Unique, high-density natural zeolite deposits have been identified which can be mined and readily processed into robust membranes for gas and liquid separations. Initial experimental results using raw, as-mined samples for gas and liquid separations show great promise for natural zeolite as a novel membrane material. Alkaline pre-treatment of the membranes improves both hydrogen selectivity and thermal stability. Two potential applications of these unique membranes, desalination and process water reclamation, were both investigated. Results of this work indicate that natural zeolites can be applied as robust membranes for gas and liquid separations. With further research, natural zeolites could serve as economically feasible membrane materials for countless industrial processes.

1.1 Zeolites and Natural Zeolites

1.1.1 Zeolites

Zeolites have been broadly named as molecular sieves. However, this definition implies their only application is 'sieving' or separation of molecules by size and only partially sheds light on the versatility and unique properties of zeolite materials. Zeolites can be categorized into three groups according to their industrial application: ion exchange, adsorption and catalysis. A number of examples are zeolites used in providing potable water via water softening, supplying purified oxygen for medical uses, and as fluidized catalytic cracking catalysts in the production of motor-gasoline [1-5]. With a myriad of applications, it is clear that zeolite molecular sieves are invaluable materials that have become integral to many industrial operations.

Classical zeolites are crystalline, inorganic materials that have a uniformly porous, three-dimensional structure resulting in a high total surface area [6,7]. Zeolites share very similar elemental compositions with quartz and feldspar materials but a comparison of specific gravity values (~2.6-2.7 for quartz and ~2.0-2.2 for zeolites) shows that zeolites have a much more open structure or framework [7,8]. Zeolite structure is formed from tetrahedrally coordinated TO_4 units, where T is either Si or Al. If the entire framework consisted of SiO_4^{4-} units then it would have a neutral charge [6,8,9]. Substituting aluminum ions into the framework, yields AlO_3^{3-}, and results in an overall negative charge on the surface. This negative charge is balanced by the inclusion of either monovalent (Li^+, Na^+,

K^+) or divalent cations (Mg^{++}, Ca^{++}, Sr^{++}, Ba^{++}) [6,9]. By ion exchange the effective pore size of the zeolites can be altered and tailored to specific separation applications. The framework aluminum sites, when exchanged with hydrogen, form strong Brønsted acid sites making them useful in catalysis [10-12].

1.1.2 Naturally Occurring Zeolites

Zeolites have been known for over two and a half centuries and initially their unique properties were only viewed as natural oddities. Axel Fredrick Cronstedt is credited with naming these minerals zeolites in 1756 deriving the name from the Greek words ζειν meaning "to boil" and λιθος meaning "stone" [8]. When these minerals are heated over a blowpipe characteristic frothing could be seen due to their high water capacity [8]. Industrial applications of natural zeolites are relatively new but have received increasing research attention over the past several decades. Modern characterisation and application of natural zeolite crystals has become an interdisciplinary study involving physics, chemistry, petrology, geology and engineering [5]. The general formula for natural zeolite frameworks is [5]:

$$(Li^+, Na^+, K^+)_a\ (Mg^{++}, Ca^{++}, Sr^{++}, Ba^{++})_d\ [Al_{(a+2d)}Si_{n-(a+2d)}O_{2n}] \bullet_m H_2O$$

The section of the formula contained in square brackets represents the tetrahedral framework of the zeolite which would have an overall negative charge [5]. Exchangeable cations are required to balance the negatively charged structure. Cations in the above formula contained in round brackets and separated by commas indicate that they are exchangeable with one another [5]. A monovalent cation can exchange with a different monovalent cation. The same is true for divalent cations. A single monovalent cation cannot replace a single divalent cation and vice versa. In order to maintain charge neutrality it requires two monovalent cations to replace a single divalent cation and vice versa. The compositions of naturally occurring zeolites vary widely with the primary compositional restriction being that Si≥Al because it is only possible to substitute every second silica in the tetrahedral framework with aluminum [6]. If this limit is exceeded the entire zeolite framework would not be able to hold its structure and would collapse. This restriction is common between natural and synthetic zeolites and is referred to as Lowenstein`s Rule.

Currently, there are well over 100 synthetic zeolites and 40 natural zeolites [8]. Naturally occurring zeolites are the most abundant authigenic silicates in sedimentary rocks and can be found readily worldwide [7,8]. Natural zeolites while offering much lower purity are being chosen over their synthetic counterparts due to widespread availability and low cost [5,8,13,14].

1.1.3 Clinoptilolite and Heulandite

The HEU framework is amongst the most common naturally occurring zeolitic frameworks [8,15]. The unit cell along (001), (100), and (010) can be seen in Figure 1. This framework has parallel 8 and 10 membered rings with an 8-member ring cross channel [7,16]. The parallel 8 and 10 member rings have pore diameters of 4.1-4.7 Å and 4.4-7.2 Å respectively [7]. The 8 member ring cross channel has a pore diameter of 4.0-5.5 Å [7]. The crystal structure is monocyclic, space group C2/m, with unit cell dimensions of a=17.7 Å, b=17.8 Å, c=7.4Å, β=116.4^{o} and Z=1 [7]. These minerals typically have a Mohs hardness of 3.5~4 [5]. Due to the difficulty of synthesizing HEU materials in the laboratory, the cheaper, less pure natural materials are typically used [16,17].

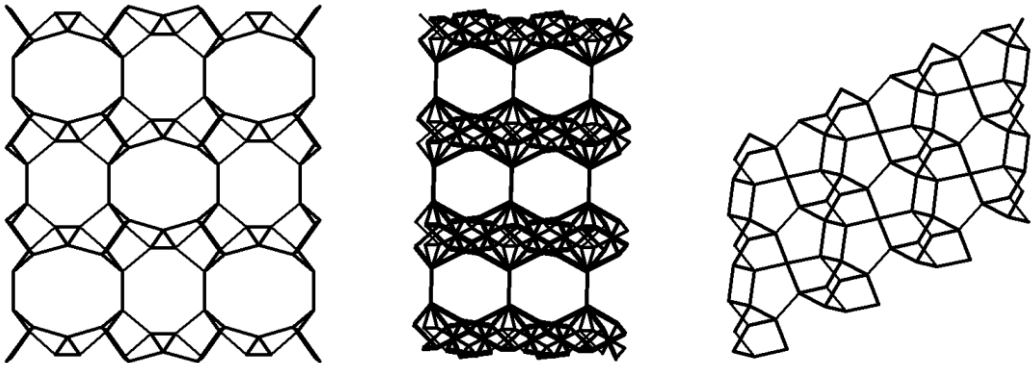

Figure 1. Unit cell structure of HEU framework as viewed from (001), (100), and (010) in (a), (b), and (c), respectively (The 3-D image of the framework of heulandite/clinoptilolite was generated using the database of zeolite structures curated by the International Zeolite Association (Ch. Baerlocher and L.B.

McCusker, Database of Zeolite Structures: http://www.iza-structure.org/databases/).)

Clinoptilolite and heulandite both exhibit the HEU framework. Heulandite was named in 1822, but was discovered much earlier and was incorrectly referred to as stilbite [5]. It was named after the English mineralogical collector H. Heuland [5]. Clinoptilolite was discovered over a century later in 1932 [13]. The first deposit of clinoptilolite from Wyoming was initially thought to be a new form of mordenite but was discovered to be a new material entirely [13]. It was given the name clinoptilolite due to its distinctive inclined edges and similarity to mordenite (ptilolite) [13]. Currently, both heulandite and clinoptilite have found widespread industrial applications due to their availability and low cost while still offering the unique properties of zeolitic materials [5,8,13]. The approximate formulas for clinoptilolite and heulandite are shown below [7]:

Clinoptilolite: $(Na^{+},K^{+})_6[Al_6Si_{30}0_{72}]\bullet_{20}H_2O$

Heulandite: $(Na^{+}, K^{+})_1(Ca^{++})_4[Al_9Si_{27}O_{72}]\bullet_{24}H_2O$

Currently, clinoptilolite and heulandite are differentiated in several different ways. Mineralogists use cationic content, declaring heulandite when

(Ca^{++}+Sr^{++}+B^{++})>(Na^{+}+K^{+}) while everything else is clinoptilolite [5,7]. While this definition does serve as an effective guideline there are deposits which do not follow this trend. Clinoptilolite has been found with high Ca^{++} and heulandites with high monovalent cationic content. Most importantly, when only the exchangeable cations are considered, it would seem that clinoptilolite can be transformed into a heulandite and a heulandite into a clinoptilolite by simple ion exchange procedures. This is simply not true. Further division is needed to characterize these two zeolites.

The Structural Commission of the International Zeolite Association (IZA) dealt with this dilemma by assigning the framework code HEU to both structures. Since heulandite was discovered first it was given priority when the framework code was assigned [19]. Now that both minerals were classified under the same framework, IZA chose to differentiate the materials based on their Si/Al ratio alone. This is effective because when ion exchange, adsorption and catalytic properties are considered it is more informative to separate clinoptilolite and heulandite by their Si/Al ratio. IZA declared that materials with a Si/Al greater than 4 are clinoptilolite and those with Si/Al less than 4 are heulandite [7,19]. Other sources have also defined the Si/Al ratio that divides clinoptilolite and heulandite to be 3.5 [20]. This method also provides better insight into the materials zeolitic properties and thermal and chemical stability.

Zeolites with high silica content can withstand exposure to higher temperatures before their framework collapses [9]. For high temperature or adsorption studies this information is much more important than knowing the

ratio of the different cations in the pores. From this viewpoint, clinoptilolite and heulandite can be separated by their thermal stability. One such definition is that the clinoptilolite framework will remain intact after overnight heating at 450 ^{o}C while heulandite's framework will collapse [13].

It is evident from the literature that determining the exact distinction between clinoptilolite and heulandite is impossible. Instead there is a continuum between these two minerals. For this study, where high temperature gas separations are investigated, clinoptilolite is required because heulandite's structure would not be able to withstand high temperatures. The most applicable differentiation between clinoptilolite and heulandite is the Si/Al ratio. Hereafter clinoptilolite and heulandite will be differentiated by their Si/Al ratio with 3.5-4 the range that separates them.

1.2 Natural Zeolite Membranes

1.2.1 Membranes and Membrane Separations

A membrane is a permselective barrier that when exposed to a driving force allows passage of specific molecules while restricting it to others [21]. This definition however oversimplifies a complex and imperative area of science. The phenomenon where a barrier preferentially allows transport of one component over another was first discovered by accident in 1748 by Nollet [22,23]. He found that a pig's bladder purified water from an alcohol/water mixture. This remained

an inexplicable mystery until Gibb's developed the concept of free energy in 1873. Since then some of the greatest researchers, such as Graham, Fick, and van't Hoff, have devoted their lives to explaining membrane transportation and revealing the many possible applications for membranes [23]. These applications are vast but some of the most important are enrichment, isolation, extraction, depletion, purification, refining, fractionation, phase separation, precipitation, volume reduction, and dehydration [22].

Membrane separations can be thought of as the process of demixing. Since the natural state of molecules is to occupy all available space and become uniformly mixed the act of demixing obviously requires energy. This energy is needed to overcome "Nature's powerful urge to equilibrate" [23]. The driving force is the source for this energy and for membrane separations it can be temperature, pressure, composition or electrical potential [22,24]. In practical applications temperature is rarely the driving force, with the exception of membrane distillation, because membrane processes are usually done isothermally [21]. Pressure difference is the backbone to almost all membrane processes by either adding pressure on the feed side (reverse osmosis, ultrafiltration, microfiltration) or reducing pressure on the permeate side (pervaporation) [21]. Processes which use concentration as the driving force include dialysis and membrane extraction. Finally, electrical potential has found specific use as the driving force in electrodialysis but is not very common otherwise [21].

Three broad classes of membrane materials exist: biological, organic (polymeric) and inorganic [21]. Among them the polymeric membranes have found the most extensive industrial use but they suffer from low thermal, mechanical and chemical stability. Cellulose acetate membranes, commonly used in water treatment, require the pH to be between 3 and 7, cannot withstand organic exposure or temperatures above $50^{o}C$ and are more susceptible to biological attack [24]. Inorganic membranes on the other hand offer extremely high thermal, chemical and mechanical stability [9].

Despite the all-encompassing drawbacks of polymeric membranes they have rooted themselves firmly into numerous industries. This is because the synthetic zeolite membranes that would be better suited for the industrial operating conditions, have shortcomings due to their support materials and synthesis procedures. The support materials, generally a sintered ceramic or a stainless steel, are porous substrates onto which the thin active layer is synthesized and they are typically very expensive in comparison to polymer membranes [24]. Synthetic zeolite membranes can be 10-50 times more expensive than their polymeric analogs [25]. The thin-films that are grown on the support surface range from several microns to approximately a hundred microns thick [9,26]. Therefore, there must be congruous chemical and physical characteristics between the support material and the synthesized active layer. If they are not compatible the active layer is more likely to detach from the support, due to poor adhesion, or crack or fracture, due to differences in thermal expansion coefficients [9]. Supported inorganic membranes are typically synthesized by dipping the

membrane into a sol-gel and pulling it out without tearing the surface layer. This is referred to as dip coating or slip casting [9]. Often a post-treatment is also required to ensure no voids are present in the thin film. This process is lengthy, tedious and the existence of a single tear or fracture makes the membrane ineffective. Also, during synthesis such factors as crystal orientation, layer thickness and quality of crystal boundaries become important. Even with all the shortcomings of the thin-film synthetic zeolite membranes they are still demanding plenty of research attention and continual developments are bringing them closer to industrial application [21,27-30].

In this study natural zeolite membranes are applied to separate hydrogen from carbon dioxide and light hydrocarbons and to separate water from ions and organic contaminants. Unique natural deposits of clinoptilolite have been identified that have extremely high densities that approach that of a single clinoptilolite crystal. These deposits exhibit essentially no macroporosity because they have been compressed over a very long time in their geographical surroundings. It has been found that these natural zeolites do not have the fragile crystal boundaries their synthetic counterparts do and therefore show great potential for large-scale industrial processes. The mechanical robustness along with extremely high thermal and chemical stability make these natural zeolite membranes show great promise for gas and liquid separations.

1.2.2 Permeation Mechanisms

How a molecule passes from the retentate to the permeate side of the membrane has been of academic interest for over a century. Many parameters control the contribution of each different transport mechanism. These parameters are temperature, pressure, molecular weight, kinetic molecular diameter, pore diameter, molecular collision-free path, heat of gas adsorption and thermal activation energies [29]. Although the applications and processes for gas and liquid separations vary greatly the mechanisms which govern the transport across the membrane are quite similar [21,26,29]. This is because on a molecular level the stages of transport across porous materials are comparable for gas and liquid molecules. Therefore, the transport mechanisms for both the gas and liquid molecules will be explained in this section with the differences highlighted throughout. The emphasis will be on gas permeation and pervaporation because those are the two membrane operations studied in this work.

In general permeation occurs in three steps: diffusion through the bulk phase to the membrane surface, mass transfer from the film adjacent to the membrane surface onto the porous material and then diffusion through the porous material [31]. The same three steps are repeated in reverse on the permeate side. The primary permeation constraints are related to the adsorption-desorption process (desorption activation energy) or due to structural constraints (configurational activation energy) [26].

For dense membranes the permeating molecule must dissolve into the membrane and transport across. These separations are based on the differences in diffusivities of the dissolved molecules and can be applied to both gases and liquids. This is called the solution-diffusion mechanism and is explained in more detail elsewhere [24]. For membranes where a porous structure exists transport is very different and several different mechanisms can be occurring simultaneously with each individual mechanism's contribution changing as operating conditions are changed. While this study does not focus on modelling or simulation analysis having a fundamental understanding of how molecules move across the membrane is needed to fully explain the experimental permeation results. The three mechanisms for molecular flow in porous media are bulk flow, molecular diffusion and molecular sieving [9,29,31,32]. A visualization of these different transport mechanisms can be seen in Figure 2.

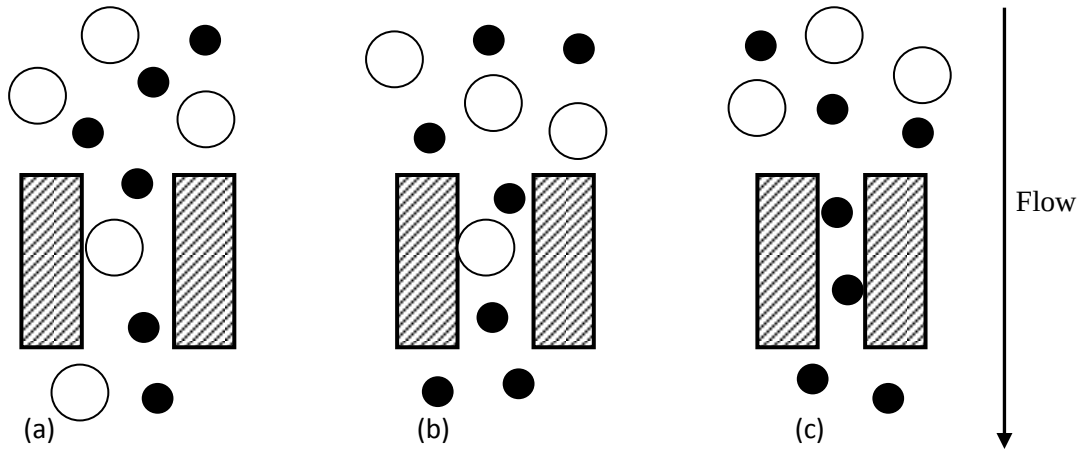

Figure 2. Visual depiction of transport mechanisms through porous media: (a) bulk flow, (b) molecular diffusion, and (c) molecular sieving (Adapted from [31]).

Bulk flow is shown in Figure 2(a) and can be described to occur when the pore opening is much larger than the molecular diameter [31]. Collisions between molecules occur more frequently than collisions between a molecule and the pore wall. When pressure is applied all molecules are able to cross the membrane freely and no selectivity is possible. Therefore, bulk flow is undesirable in membrane separations. Molecular diffusion, shown in Figure 2(b), occurs when pressure is equal on both sides of the membrane and transport is due to a gradient in fugacity, activity, chemical potential, concentration or partial pressure [31]. When a sweep gas is used on the permeate side even when a pressure gradient is applied some permeation will be due to molecular diffusion because of a partial pressure gradient. For zeolites the ideal membrane would operate purely via molecular sieving, shown in Figure 2(c). When the pore diameter is between the molecular diameters of at least some of the molecules size exclusion separations are possible. This type of transport has also been referred to as ‘molecular sieving’ [31]. For gas separations if permeance increases with increasing temperature it is assumed that activated diffusion is occurring.

Theoretically, a perfect zeolite membrane could offer 100% selectivity via molecular sieving. In practice though, creating a perfect zeolite membrane is not possible. All three transport mechanism depicted in Figure 2 are occurring

simultaneously for natural zeolite membrane separations because a large range of pore sizes are present. Even when pressure is applied molecular diffusion still contributes and when intercrystalline voids are present bulk flow could dominate. In general for natural zeolites, high density is indicative of strong grain boundaries and fewer macropores, increasing the contribution of molecular sieving.

A special case of gas permeation for microporous materials is called Knudsen diffusion. Knudsen diffusion occurs when the pore diameter is large enough to allow both molecules to enter but the mean free path of the gas molecules is greater than the pore diameter [31]. In this case collisions with the pore walls occur more frequently than collisions between molecules. For Knudsen diffusion, selectivity is limited and is represented by the ratio of the component's Knudsen diffusivities. Knudsen selectivity can be simplified to a ratio of the inverse squares of the molecular weights as shown in the following formula:

$$S_{ij} = \frac{\sqrt{M_j}}{\sqrt{M_i}} \quad (1)$$

where S_{ij} is the selectivity of component i over component j and M is the molecular weight of either component i or j. Knudsen selectivities are used as a benchmark in the gas permeation experiments in this study. Selectivities above Knudsen indicate separation by porous zeolite materials in the mineral rather than non-selective transport through defects or intercrystalline voids. Knudsen separation selectivities of H_2 over CO_2, CH_4, C_2H_4 and C_2H_6 are 4.69, 2.83, 3.74, and 3.87 respectively. Bulk and Knudsen diffusion are commonly described

together using the dusty gas model instead of assuming that one mechanism dominates the other. A thorough explanation of the dusty gas model can be found in literature [32,33].

Concentration polarization is a phenomenon that can have a profound effect on permeation and selectivity, especially in pressure driven processes. Concentration polarization occurs when a membrane is permeable to one molecule but not another and the non-permeating molecule accumulates at the membrane surface, increasing its concentration to considerably higher levels than in the bulk [22,31,34]. A visualization of this effect can be seen in Figure 3. Factors that can cause the onset of concentration polarization are low viscosity, low flow rate, low concentration of the permeating molecule, fouling and the design of the membrane module. Studies have shown that by adding spacers near the membrane surface this accumulation can be minimized [35]. Also, by having the feed flowing in a cross flow pattern the non-permeating molecules are more likely to be carried away instead of concentrating at the membrane surface.

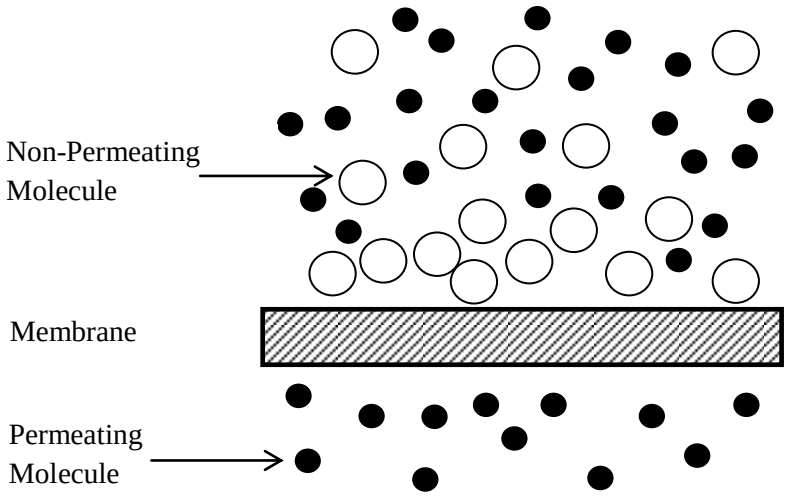

Figure 3. Visual depiction of the concentration polarization effect.

1.3 Gas Membrane Separations

Hydrogen is the most abundant element in the universe but rarely occurs in its free state on Earth [36]. Henry Cavendish in 1766 first identified hydrogen only as ‘inflammable air’. In 1783, Antoine-Laurent Lavoisier noted that when ‘inflammable air’ was combusted water was formed [36]. Thus, hydrogen received its name from the combination of the Greek words ‘*hydro*’ and ‘*genes*’, which translates to ‘maker of water’ [36]. Hydrogen has become one of the most important feedstocks in the chemical industry and in refineries [37]. A large amount of hydrogen is used in the production of ammonia and methanol. Pure hydrogen is a common feedstock in production of consumer goods such as edible oils, cosmetics, vitamins, soaps, lubricants and even peanut butter [37]. In refineries hydrogen is needed in upgrading processes, such as hydrotreating and

hydrocracking, to remove impurities such as sulfur, nitrogen and heavy metals. Hydrogen's roles at refineries will become even more important as increasingly contaminated crude oils are being refined. Hydrogen is also receiving much attention as a clean, zero-emission fuel candidate. The demand for hydrogen is expected to grow by 10-15% annually for the foreseeable future [38].

Every year 41 million tons of hydrogen is produced by steam reforming, partial oxidation and autothermal or oxidative steam reforming [39]. In some niche markets hydrogen is also produced by electrolysis, but this method has not found large-scale application. Over 80% of hydrogen generation is by steam reforming [39]. Steam methane reforming yields the highest amount of hydrogen but also requires the highest amount of energy because it's endothermic. These processes yield syngas, a mixture of hydrogen, carbon monoxide and carbon dioxide, and therefore require further separation if pure hydrogen is the desired feedstock [36,37]. Water gas shift reactions are commonly employed to convert the carbon monoxide into carbon dioxide and more hydrogen [36].

Syngas can be separated into its components using pressure swing adsorption (PSA). At high pressures, up to 4MPa, the carbon dioxide is adsorbed on zeolites, activated carbon, silica or alumina gels and the hydrogen is collected [36]. The adsorbent is regenerated by desorbing the impurity gas at low pressures. High purity hydrogen, up to 99.999%, with overall recovery of approximately 90% can be efficiently produced by this method [36]. Although, the explanation seems simplistic, in practice multicolumn adsorption systems under cyclic steady state operation are very complex and although PSA does efficiently scale-up, it

does not scale down effectively. It is estimated that a 20% improvement in the separation and purification of the hydrogen would yield an energy savings of 450 trillion BTU per year [39].

Since 2000 over 430 patents have been issued pertaining to advances in hydrogen selective membranes [39]. Membrane separation could provide a single pass hydrogen producing process that does not require varying temperature or pressure to regenerate adsorbents. The most desirable hydrogen selective membrane would be resistant to sulphur and steam and have high thermal stability. Dense palladium membranes have been shown to purify hydrogen but the high cost of palladium and its alloys restricts their application in industry. Natural zeolite membranes could potentially offer a viable alternative in the production of purified hydrogen.

1.4 Liquid Membrane Separations

Currently, there are approximately 1,400 million km^3 of water on Earth, 35 million km^3 of which is freshwater primarily found as permanent ice or snow in Antarctica and Greenland, or in deep aquifers [40]. Humans get water from lakes, rivers, soil moisture and shallow groundwater reservoirs accounting for about 200,000 km^3 of freshwater, or less than 1% of the world's freshwater [40]. It can be seen in Figure 4 that this available freshwater is not distributed evenly throughout the planet. Over 60% of the 227 natural rivers have already been dammed causing between 40-80 million people to relocate and causing

irreversible damage to the environment [40]. Demand for fresh water has been increasing and will continue to do so. Between the years of 1972 to 1991 water consumption increased by 80% while total population only increased by 3% [40]. Generated wastewater alone increased from 47 to 125 million m^3 per year from 1985 to 1995 [41]. It is estimated that between 1995 and 2025 the annual water volume used in industry will increase by 50% [41]. As freshwater is becoming increasingly scarce in many areas around the world the desalination of seawater and the reclamation of industrial process water is expected to take on greater significance. These two areas, desalination and reclaiming process water, are the focus of the natural zeolite membrane liquid separations conducted in this study.

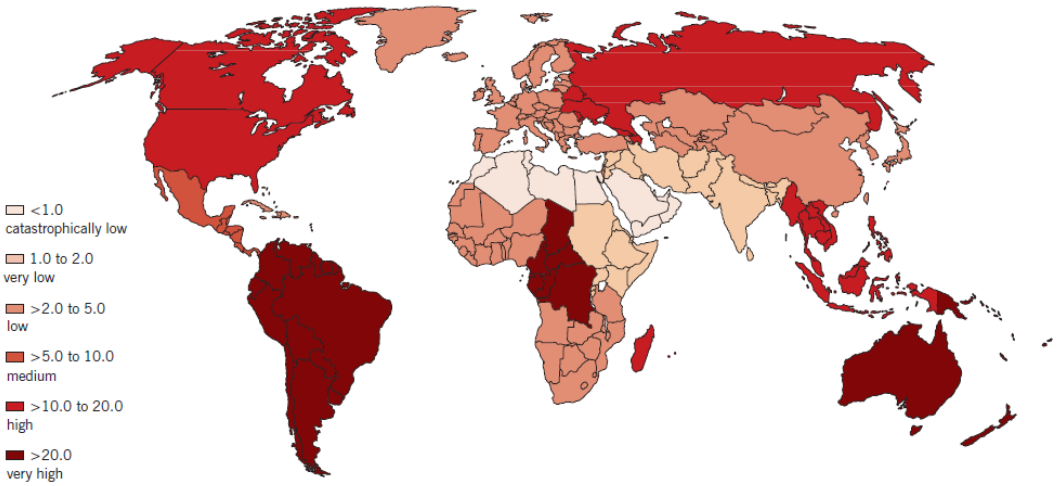

Figure 4. Global availability of freshwater in 2000 at 1,000m^3 per capita per year [40].

Modern desalination by reverse osmosis using polymeric membranes is a well-established and well-recognized technology [42,43]. Desalination is not only required for the generation of potable water but is also needed in many industries, including power generation, glass manufacturing, electronics, pulp and paper, textiles, and cooling systems [41]. As discussed earlier though, polymeric membranes suffer from poor chemical and physical stability. Therefore, due to fouling or breaking, desalination membranes must be replaced often. Because of their poor chemical resistance membrane regeneration using harsh chemicals is not an option. There is a global demand for low cost, high efficiency desalination technologies and zeolites show great potential for this application.

Currently, pervaporation is being considered for desalination processes, even though most industrial desalination is conducted via reverse osmosis [44-47]. Simulation experiments conducted by Lin et al. showed 100% Na^+ rejection through a perfect zeolite A crystal lattice under reverse osmosis operation [48]. Cho et al. used a NaA zeolite membrane for the desalination of a synthetic seawater and reported that at 69 ^oC a water flux of 1.9 kg/m^2h and ion rejection over 99.9% was achieved [49]. In some studies the permeate water is approaching that of the purity of ultrapure water [50]. Using actual North Sea water and hydroxy sodalite pervaporation membranes ion rejections over 99.99% were achieved [50].

A natural extension of the desalination work is using natural zeolite membranes to reclaim process water. This would have a profound impact on the oil sands industry where bitumen extraction is performed using hot water.

Bitumen is a high molecular weight, high viscosity, contaminated analog of crude oil that can be recovered and refined into a synthetic crude oil [51]. This synthetic crude oil can then be refined into carbon based fuels and products such as gasoline and diesel fuel. In Alberta alone there are 169.7 billion barrels of remaining established bitumen reserves with 135.5 billion barrels accessible only by in situ methods [51]. The remaining bitumen reserves are economically suitable for mining techniques. Since 1967, when crude bitumen production began in Alberta, approximately 4% of the initial established reserves have been extracted [51]. By 2015 it is predicted that in situ bitumen production in Alberta will surpass surface mining production [51].

Steam assisted gravity drainage (SAGD) was developed by Roger Butler with Imperial Oil in the late 1970's and is currently the leading method of in situ bitumen production [52]. Since at reservoir conditions bitumen will not flow, in SAGD production steam is injected into deep oil sands formations. This heats the bitumen, lowering its viscosity, so it will flow and can be recovered. The steam to oil ratio (SOR) is typically used to gauge SAGD operation performance and is in the range of 2-6 [53]. Therefore, 2-6 barrels of water are needed as steam for every 1 barrel of oil produced. Great difficulty lies in reclaiming the contaminated process water once the bitumen has been removed. Several processes are required to ensure the process water is of boiler quality and can be vaporized and injected back into the well [54-56]. A generalized block diagram of this process can be seen in Figure 5. Organics and some of the ionic content is removed by lime softening [54]. Suspended solids are removed by filtration. The ionic content must

be especially low otherwise scaling will occur in the steam generator. Weak acid cation exchange removes residual ions and provides boiler quality water [54]. A continuous, single-pass natural zeolite membrane process could remove organics, silica and ions while offering the thermal and chemical stability that currently restricts polymer membrane processes for purifying process waters.

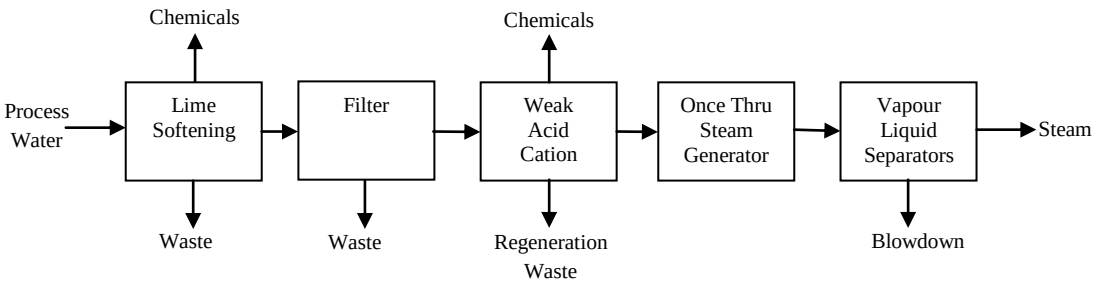

Figure 5. Block diagram of typical process scheme for recovering contaminated SAGD process water (Adapted from [54]).

Chapter 2. Material and Methods

2.1 Natural Zeolite Characterisation

2.1.1 X-Ray Diffraction

To give qualitative insight into the crystal structures and their purity, x-ray diffraction (XRD) was used. XRD can effectively determine which zeolitic frameworks and impurities are present. When modifying or upgrading the surface

of natural zeolites XRD is a quick and efficient method for determining what crystal frameworks are being formed or destroyed. An XRD pattern, before and after modification, can be analyzed for peak shifts, changes in peak intensity and peak formation or destruction. It should be noted that XRD is not always effective at differentiating between different zeolite materials that share the same framework. For example, the HEU framework is shared between clinoptilolite and heulandite, as previously mentioned. A Rigaku Gigerflex 2173 with Co tube and a vertical goniometer equipped with a graphite monochromator was used for all XRD characterisation. XRD patterns were compared to data available from the International Center for Diffraction Data-Powder Diffraction File (ICDD-PDF) along with visual comparisons to existing standards and literature.

2.1.2 Scanning Electron Microscopy

Visual inspection of the surface for cracks and fractures that may have propagated though the zeolite during excavation was done for every sample. This reveals obvious impurities or cracks but does not reveal anything about the surface properties on a micron-scale, such as surface homogeneity, macroporosity and crystal size. Scanning electron micrographs (SEM) were taken at several different magnifications. When using a natural zeolite as a membrane it is crucial to make sure there are no pinholes or macroscopic voids in the surface. If these exist in the membrane surface the zeolite won't provide effective separation for

gases or liquids. Scanning electron micrographs were conducted using a JEOL 6301F field emission scanning electron microscope.

2.1.3 Electron Dispersive X-Ray Microscopy

Energy dispersive x-ray spectroscopy (EDX) is typically done simultaneously with SEM to obtain the surface elemental composition. An elemental analysis of zeolitic materials is vital during characterisation of the HEU framework. Since, as the Si/Al ratio changes, the HEU framework varies from heulandites to clinoptilolite. These two forms of the HEU framework have very different properties, such as temperature stability and cation exchange capacity, so understanding which form is present is important. EDX can also confirm what cations are naturally present in the zeolite pores which can influence subsequent ion-exchange and surface modification treatments. The one limitation of EDX is that it only provides elemental analysis of the surface and not the entire material. While this isn't detrimental it is noteworthy. EDX was done at an acceleration voltage of 20kV using a liquid nitrogen-cooled, lithium drifted silicon detector equipped with a Norvac window (Princeton, Gamma-Tech).

2.1.4 BET Specific Surface Area Measurements

Nitrogen adsorption isotherm data was obtained with a Quantachrome Instruments AUTOSORB-1 with an activation temperature of 250 ^{o}C. The zeolite

surface areas were then calculated using the Brunauer, Emmett and Teller (BET) method. By comparing the determined surface areas to values found in literature, conclusions pertaining to zeolite purity can be made. In the natural form the cations in the zeolite pores are typically Na^{+}, Ca^{++}, Mg^{++}, K^{+} and they could be restricting N_2 access to the internal surfaces of the zeolite by blocking the pores. Therefore, nitrogen adsorption measurements were also done on samples that had been ion-exchanged into the hydrogen ion form. First, the natural zeolites were exchanged with ammonium nitrate at 80 ^{o}C for 16 hours. The ion exchange solution ratio of NH_4NO_3, natural zeolite, and deionised water was 2:1:10 by weight. To ensure complete exchange, the exchange was repeated 3 times. By calcining the sample the zeolite undergoes the following reaction:

$$NH_4^{+}{}_{(zeolite)} \leftrightarrow H^{+}{}_{(zeolite)} + NH_{3(g)}$$

The NH_3 gas is swept away by a nitrogen sweep gas in a Thermolyne 79400 Tube Furnace. Several different calcination temperatures were used with higher temperatures favouring the forward reaction but at the risk of damaging the zeolite structure. Every natural zeolite sample for surface area measurements was also submitted to XRD to ensure the zeolite framework had not been damaged.

2.2 Gas and Liquid Permeation Experiments

2.2.1 Gas and Liquid Membrane Preparation

Gas separation membranes were made from a clinoptilolite-rich deposit from Castle Mountain zeolites (Quirindi, NSW, Australia). Liquid separation membranes were prepared from a natural zeolite deposit in Mt. Kobau and Manery Creek area of British Columbia. Photographs of both natural zeolites along with their respective membranes can be seen in Figures 6 and 7. The natural zeolite samples were received as large untreated pieces and were sectioned into thin slices using a Rock Rascal Model TM Combination Trim Saw/Grinder equipped with a MK USA MK-303 diamond lapidary saw blade. The membranes were polished to their desired thicknesses using a 180-grit rotating diamond lapidary disc. Gas separation membranes were 1.0-1.5 mm thick with 1.25 cm diameter. Liquid separation membranes were 2.0-2.4 mm thick and were 2.5 cm by 3.5 cm. Gas membranes were sonicated for 30 minutes in an ultrasonic bath then dried at 120 ^{o}C for at least 2 hrs. Liquid membranes were rinsed thoroughly with deionised water and were dried at ambient conditions for 16 hours.

Figure 6. Castle Mountain natural zeolite and gas separation membranes.

Figure 7. British Columbia natural zeolite and a liquid separation membrane.

2.2.2 Gas Permeation Experiment

Figure 8 shows the gas permeation experimental set-up. The membrane was sealed to the top of a ceramic tube with an outer diameter of 0.5 inches. Heraeus SG-683K glass sealant was used to seal the membrane to the ceramic tube. The glass sealant was applied to the joint and was dried at 150 ^{o}C for 10 minutes, heated to 650oC at 1^{o}C/min where it was kept for 10minutes then cooled to ambient temperature at 1^{o}C/min. All increases and decreases in the temperature were done at 1 ^{o}C per minute to avoid thermal shock. The feed side was a quartz tube and the permeate side was a ¼ in. ceramic tube inside a ½ in. ceramic tube

where a sweep gas carried the permeate away. The feed gas (H_2, CO_2, CH_4, C_2H_4, C_2H_6) and the sweeping gas (Ar) flow rates were kept at 100 mL/min (STP) and 200 mL/min (STP), respectively. The parts of the experimental set-up that were inserted directly into the tube furnaceare shown in Figure 8. Experiments were done at approximately 100 kPa partial pressure difference as temperature was increased from 25 °C to 500 °C. All gases used were provided by Praxair Canada. Swagelok fittings and valves were used for the entire set-up. Gas composition of both the feed and outlet permeate were analyzed with a Shimadzu GC-14B with a HayeSep Q packed column equipped with a thermal conductivity detector.

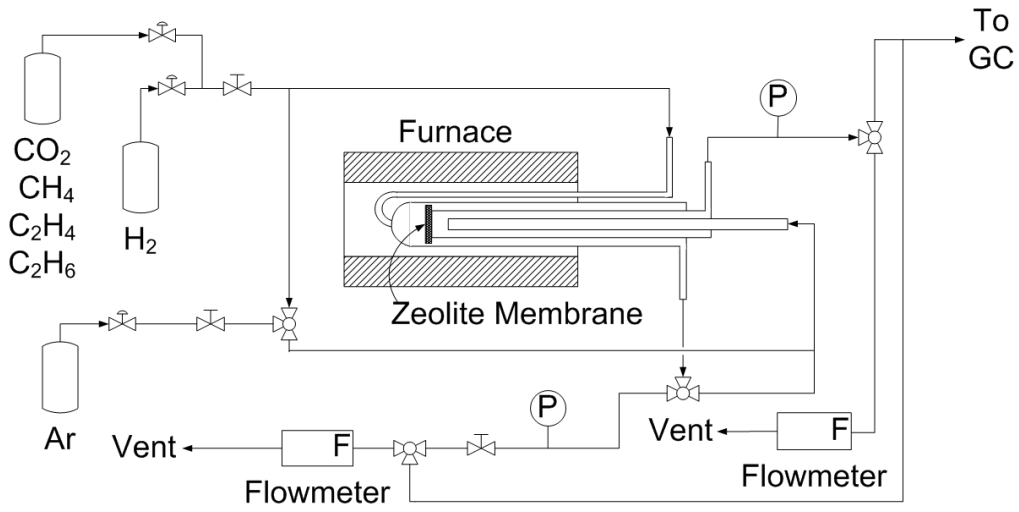

Figure 8. Schematic of the gas permeation experimental set-up.

The two values calculated and analyzed during gas permeation experiments were permeance and ideal selectivity. The permeance can be defined

as molar flux divided by partial pressure difference with units of mol/area/time/pressure. It is calculated using the following formula:

$$P_i = \frac{N_i}{\Delta p_i} \quad (2)$$

where P_i is the permeance (mol m^{-2} s^{-1} Pa^{-1}), N_i is the molar flux (mol m^{-2} s^{-1}), and Δp_i is the partial pressure difference (Pa). All three terms are with respect to component i in the system. All experiments conducted were single component systems and the calculated selectivities were therefore ideal selectivities and not selectivities of their corresponding multi-component systems. Ideal selectivity was calculated using the following formula:

$$S_{ij} = \frac{P_i}{P_j} \quad (3)$$

where S_{ij} is the ideal selectivity of component i over component j.

Gas separation membranes underwent further modification to increase flux and selectivity. The treatment used was intended to tailor the properties of the natural zeolite surface and fill intercrystalline voids leaving only the zeolitic channels available for permeation. A visualization of the surface modification process can be seen in Figure 9. In the centre of a Teflon lined autoclave a gas separation membrane, prepared as described above, was placed on top of a glass vial. A small amount of deionised water was added inside the glass vial and to the surrounding area such that the membrane itself never comes into contact with the liquid water. The set-up of the membrane surface modification can be seen in Figure 10. The surface modification solution was a mixture of sodium silicate,

sodium hydroxide, and deionised water with a weight ratio of 5:1:14. Two drops of the surface modification solution were added to the top of the gas membrane and the autoclave was sealed and heated to 150 ^{o}C for 3 days. After three days the membrane was removed from the autoclave, rinsed with deionised water, polished with 400 mesh silicon carbide sand paper then rinsed again with the deionised water. Finally, the membrane was re-dried at 120 ^{o}C for 2 hrs.

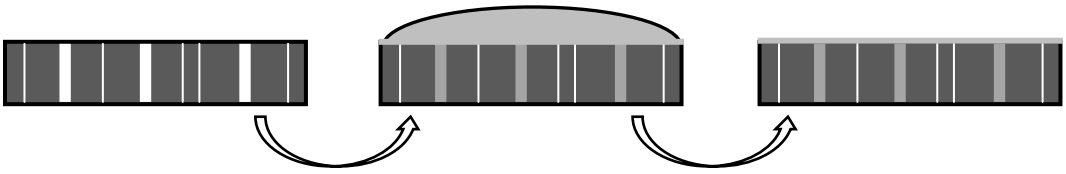

Figure 9. Visualization of the surface modification of natural zeolite gas membranes.

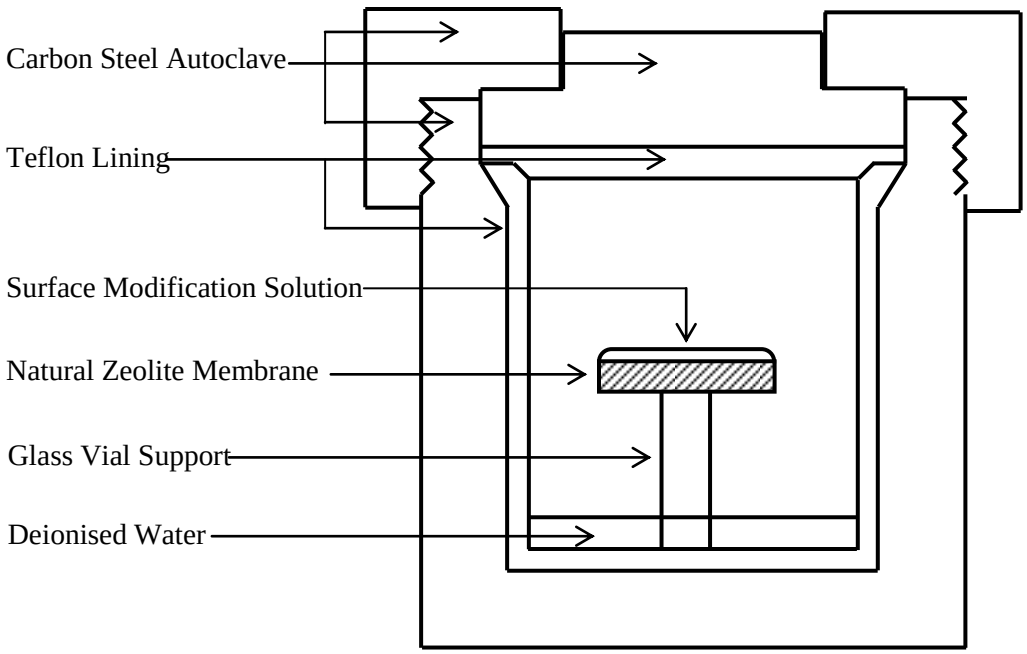

Figure 10. Membrane surface modification autoclave set-up.

2.2.3 Liquid Permeation Experiment

A schematic of the liquid permeation experimental set-up can be found in Figure 11. Two identical membrane cells were made out of Plexiglas and stainless steel for waters containing and not containing organics, respectively. The effective membrane area for each was approximately 6 cm^2 with a constant feed flow rate of 1 L/min. To minimize the effects of concentration polarization the bath water was circulated in a cross-flow pattern. The bath water and the retentate stream temperatures were monitored by two J-Type thermocouples. The bath water temperature range investigated was 25 ^oC to 93 ^oC with temperature drop between the bath and the membrane cell never exceeding 2 ^oC. The base water used for all experiments was City of Edmonton municipal water. This water was

used to establish a baseline flux before the addition of salts or organics. Hereafter, it will be referred to as baseline water.

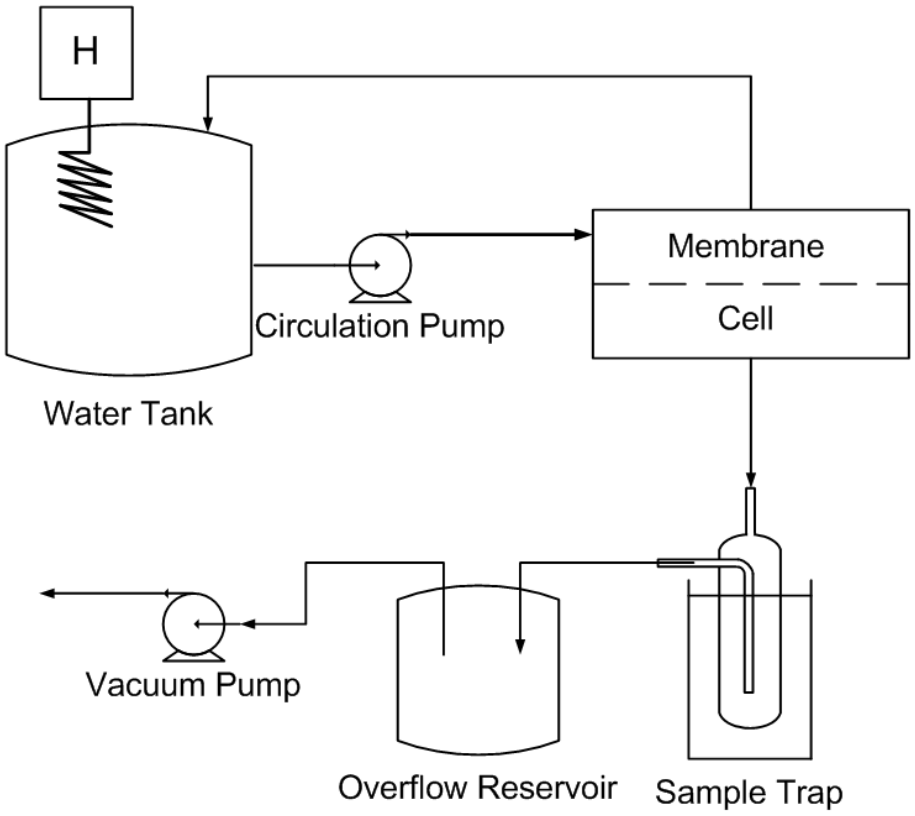

Figure 11. Schematic of the liquid permeation experimental set-ups.

For the initial proof of principle experiments only the ionic content was monitored. For these experiments the temperature was controlled digitally using a Fisher Scientific Isotemp 3013HS Circulating Bath. In the Plexiglas cell the natural zeolite membranes were sealed into place using Permatex Ultra Copper

instant gasket sealant. The cold trap used for these experiments was a mixture of dry ice and ethanol at approximately -70 ^{o}C. For single compound permeation experiments NaCl (≥99.0% purity, Sigma-Aldrich) was added at varying concentrations. Sea salts (Sigma-Aldrich) were used to make a synthetic seawater using the directions provided (3.8 g/L). Feed and permeate ionic concentrations were measured using a Varian 220FS Atomic Absorption Spectrometer. An air-C_2H_2 flame was used for analyzing Na^+, K^+, and Mg^{2+}, and an N_2O-C_2H_2 flame was used for Ca^{2+}.

The stainless steel membrane cell was used to run initial experiments with synthetic process water. The synthetic process water was made using the Sea Salts at a lower concentration with the addition of ACS Certified Toluene from Fisher Scientific. Toluene was chosen to be the model organic compound because it is likely to be one of the smallest organics found in contaminated process waters. The Permatex Ultra Copper instant gasket sealant isn't suitable for organic exposure so West System 105 Epoxy Resin and 205 Fast Hardener were used. West Systems 2-part sealant is suitable for higher temperatures and is more chemically resistant to organics than Permatex but is not viscous enough on its own so natural zeolite powder was mixed in to form a sealant paste. To ensure no permeation was occurring a membrane made entirely of the sealant-zeolite paste was tested and was found to have no cross membrane flux. Temperature was controlled and monitored using a Heetgrid Immersion Heater and was monitored using J-Type thermocouples. The bathwater was circulated using a Hydra Cell Pump CFW10 EasyDrive equipped with a Blacoh Fluid Control Dampener with

an EPDM Diaphragm. Due to the high volatility of the toluene in the permeate, a dry ice and diethyl ether cold trap at approximately -90 ^{o}C was used to ensure all toluene was collected. The ionic content was again measured using the Varian 220FS Atomic Absorption Spectrometer. A Hewlett-Packard Series II 5890 gas chromatograph with a flame ionization detector (GC-FID) was used to measure organic concentrations.

A summary of the differences between the two water cells can be found in Table 1.

Table 1. Comparison of liquid permeation experimental set-ups.

Experiment	**Desalination**	**Process Water Reclamation**
Cell Material	Plexiglas	Stainless Steel
Bath Water Contaminant	NaCl or Sea Salts	Sea Salts and Toluene
Temperature Control	Fisher Scientific Isotemp 3013HS Circulating Bath	Heetgrid Immersion Heater
Flow Control	Fisher Scientific Isotemp 3013HS Circulating Bath	Hydra Cell Pump CFW10 EasyDrive equipped with Blacoh Fluid Control Dampener with a EPDM Diaphragm
Sealant	Permatex Ultra Copper Instant Gasket	West System 105 Epoxy Resin and 205 Fast Hardener with added natural zeolite powder
Permeate Characterization	Atomic Absorption	Atomic Absorption GC-FID
Cold Trap	Dry Ice/Ethanol	Dry Ice/Diethyl Ether
Cold Trap Temperature	~ -70 ^{o}C	~ -90 ^{o}C

Before all pervaporation experiments vacuum was applied to the permeate side for 30 minutes in order to collect any residual water on the permeate side, possibly left from the previous day's experiment or water that may have

permeated during the heating of the bathwater. 30 minutes was determined to be sufficient to remove all residual water on the permeate side. Because the Plexiglas cell and stainless steel cell are of identical design it was assumed that 30 minutes was also enough time for the stainless steel cell. The cold trap was rinsed three times thoroughly, interior and exterior, with deionised water and was dried completely in an oven at 100 °C. All liquid permeation runs were 1.5 hours long. The glass cold trap was removed from its cooling solution and allowed to equilibrate with ambient conditions. For experiments with toluene the glass cold trap was sealed by connecting the outlet and inlet with plastic tubing so the toluene could not escape. By weighing the glass cold trap before each run and after each run, once equilibrated with ambient, the amount of liquid sample collected was measured and used to calculate flux. Flux was calculated using the following equation:

$$F = \frac{W}{t \times A \times 1000} \quad (4)$$

where F is flux (kg m^{-2} hr^{-1}), W is the weight of the sample collected (g), t is the run length (hr) and A is the effective membrane area (m^2).

Chapter 3. Results and Discussion

3.1 Gas Separations

3.1.1 Natural Zeolite Characterization

Initial investigations into natural zeolite membranes were performed using a high density clinoptilolite from Castle Mountain, Australia and were focused on separating hydrogen from carbon dioxide and light hydrocarbons. The measured bulk density was determined to be approximately 2.7 g/cm^3. This high density could be indicative of impurities but it was determined that the Castle Mountain deposit is actually high purity clinoptilolite with essentially no macroporosity and strong crystal boundaries [15]. Scanning electron micrographs of the raw, unpolished, untested Castle Mountain zeolite are presented in Figure 12. The platy morphology with inclined edges, typical of clinoptilolite crystals, can be seen throughout the entire surface of the Castle Mountain membrane. Due to unique geographical history this mineral has been compressed removing intercrystalline voids and increasing its mechanical strength [15]. No large gaps or defects can be seen in the surface of the as-mined Castle Mountain membranes which can help decrease or eliminate the contribution of bulk flow to overall permeation.

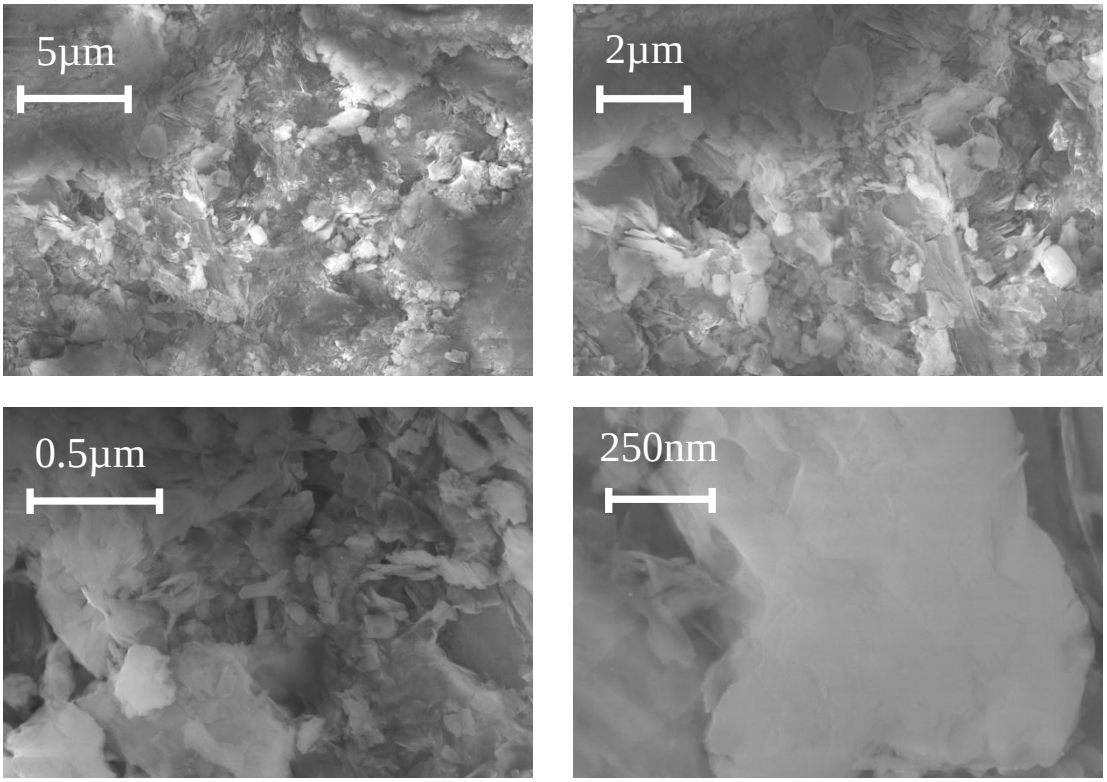

Figure 12. Scanning electron micrographs of raw, unpolished, untested Castle Mountain clinoptilolite.

XRD patterns for both the raw and upgraded Castle Mountain membranes are presented in Figure 13. The characteristic 2θ peaks of the HEU framework are marked with stars. The dominant impurity detected in both XRD patterns is mordenite. Mordenite is a thermally stable zeolite with an effective pore diameter of approximately 5Å; comparable to the largest pore in the clinoptilolite structure. Trace amounts of quartz (SiO_2) were detected and could indicate high silica content throughout the mineral. This implies that the HEU framework likely has a high Si/Al ratio making it a clinoptilolite rather than heulandite. For gas

separations where high thermal stability is required clinoptilolite would be the preferred zeolite membrane. Despite the upgrading process using high concentrations of caustic the clinoptilolite framework is still present in the upgraded XRD pattern. The main changes in structure are in the 2θ range of 15-40^{o}. After upgrading, peaks at 15.8^{o} and 32.3^{o} increased while peaks at 22.1^{o} and 27.6^{o} decreased. The 2θ where these changes occur are not characteristic peaks of the HEU framework and represent a new crystalline phase being formed during the upgrading procedure [15]. The surface morphology of the clinoptilolite surface does not change substantially after upgrading. SEM micrographs of the membrane surface before and after upgrading are presented in Figure 14.

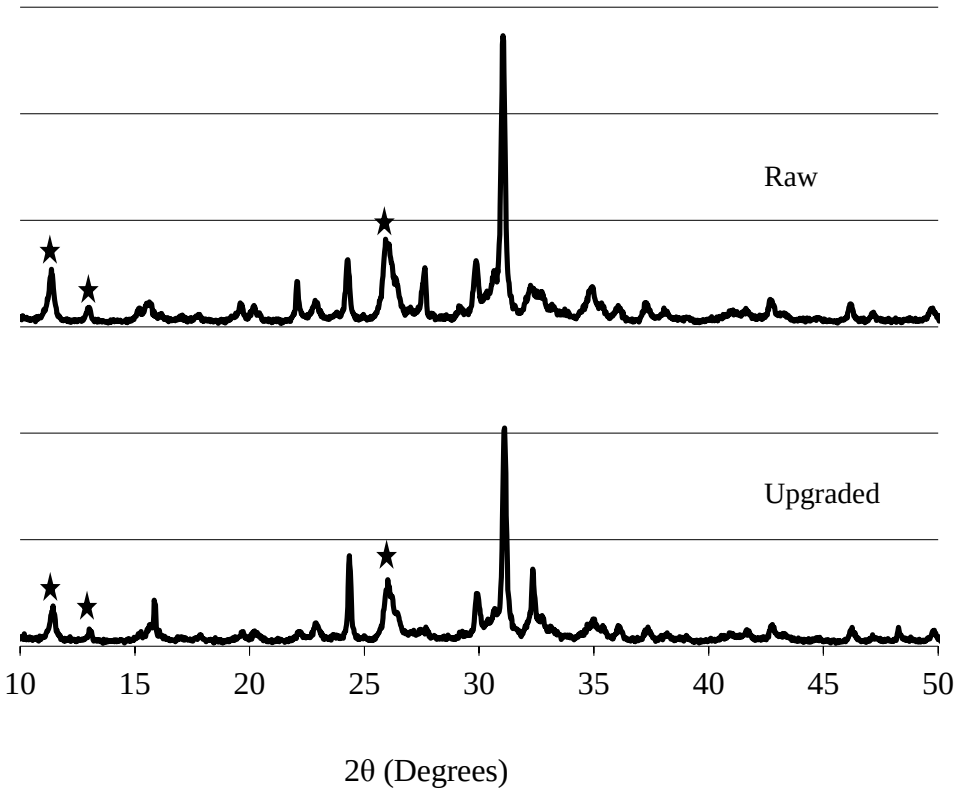

Figure 13. XRD patterns for raw and upgraded Castle Mountain clinoptilolite membranes.

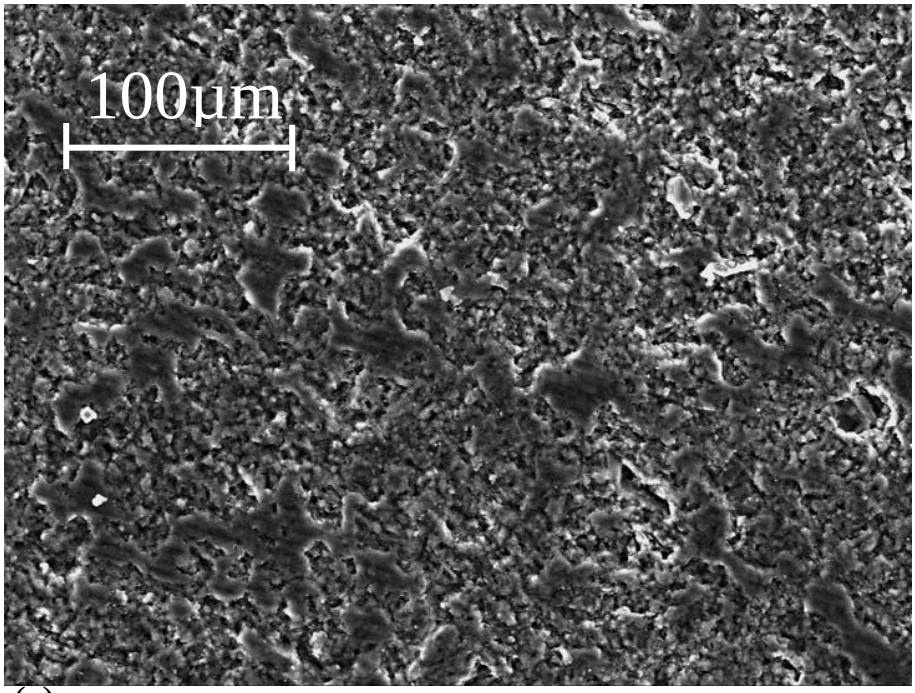

(a)

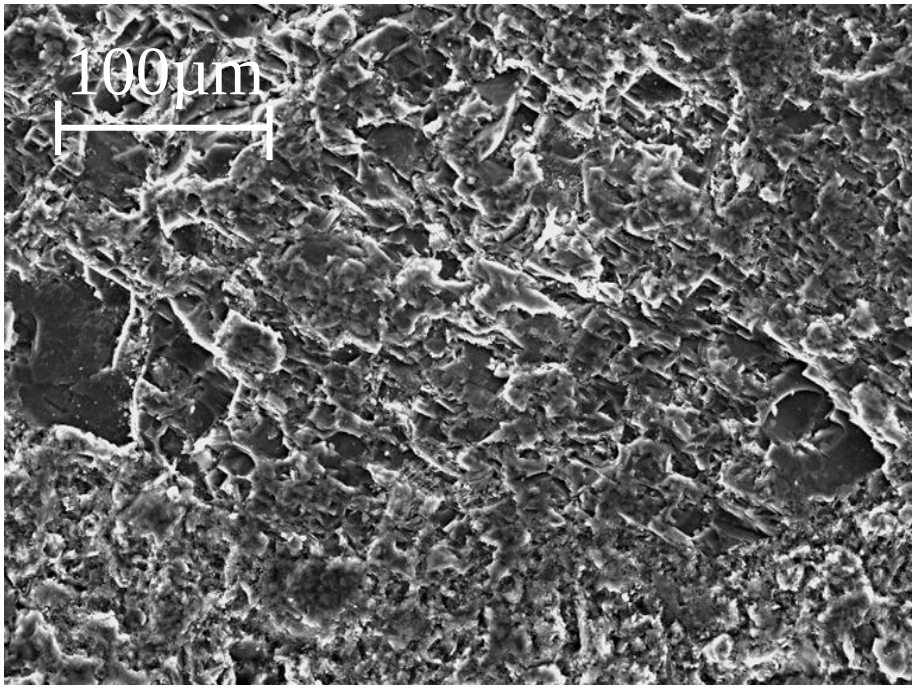

(b)

Figure 14. SEM images of the surface of the Castle Mountain clinoptilolite membranes (a) before upgrading and (b) after upgrading.

The manufacturer advertises Castle Mountain zeolite as being approximately 85 wt% clinoptilolite, 15 wt% mordenite with trace impurities of quartz. Manufacturer provided mineralogical composition for the Castle Mountain zeolite is presented in Table 2. The calculated Si/Al ratio from the manufacturer provided data in Table 2 is 5.03. EDX elemental analysis of the membrane surface before and after upgrading was performed. The Si/Al ratio determined from EDX for the raw and upgraded membranes was 9.17 and 7.49, respectively. Also, both Si/Al ratios are substantially higher than 5.03. The decrease in Si/Al is most likely due to dissolution of impurities containing silica during the surface modification [15]. It is noteworthy that the elemental composition of the membrane surface varied which is consistent with the variability in natural zeolite minerals.

Table 2. Mineralogical composition of Castle Mountain clinoptilolite provided by the manufacturer.

Mineral Content	**Weight Percent**
SiO_2	71.81
Al_2O_3	12.10
Fe_2O_3	1.14
Na_2O	2.33
K_2O	0.90
CaO	2.60
MgO	0.65
TiO_2	0.22
MnO	0.03
P_2O_5	<0.01
SrO	0.22

The SEM images, XRD patterns, mineralogical data, and EDX elemental analysis all show that Castle Mountain is a high purity clinoptilolite with minor mordenite impurities exhibiting virtually no macroporosity or intercrystalline defects. Castle Mountain zeolite can be considered as a robust, mechanically and thermally stable clinoptilolite with inherent characteristics that are desirable for a hydrogen selective membrane.

3.1.2 Gas Permeation Experiments

Gas permeation results for the raw clinoptilolite membranes showed relatively stable fluxes and selectivities above Knudsen. The permeation results for H_2, CO_2, CH_4, C_2H_4, and C_2H_6 across a raw clinoptilolite membrane are presented in Figure 15. The average H_2 permeance across the entire temperature range is approximately 2.5 x 10^{-7} mol/(m^2·s·Pa). All permeances are the average of three runs on the same membrane. Above 100 ^oC standard deviations remained below 20%. The low concentrations of the gases in the permeate can be assumed to contribute to unstable permeances [15]. Permeance variability for all gases across as-mined membranes is expected due to impurity content and composition differences between the samples. While the clinoptilolite framework is stable at the experimental temperatures there is the potential for phase transformation of impurities above 400 ^oC. This may be a contributing factor to permeance variability as well.

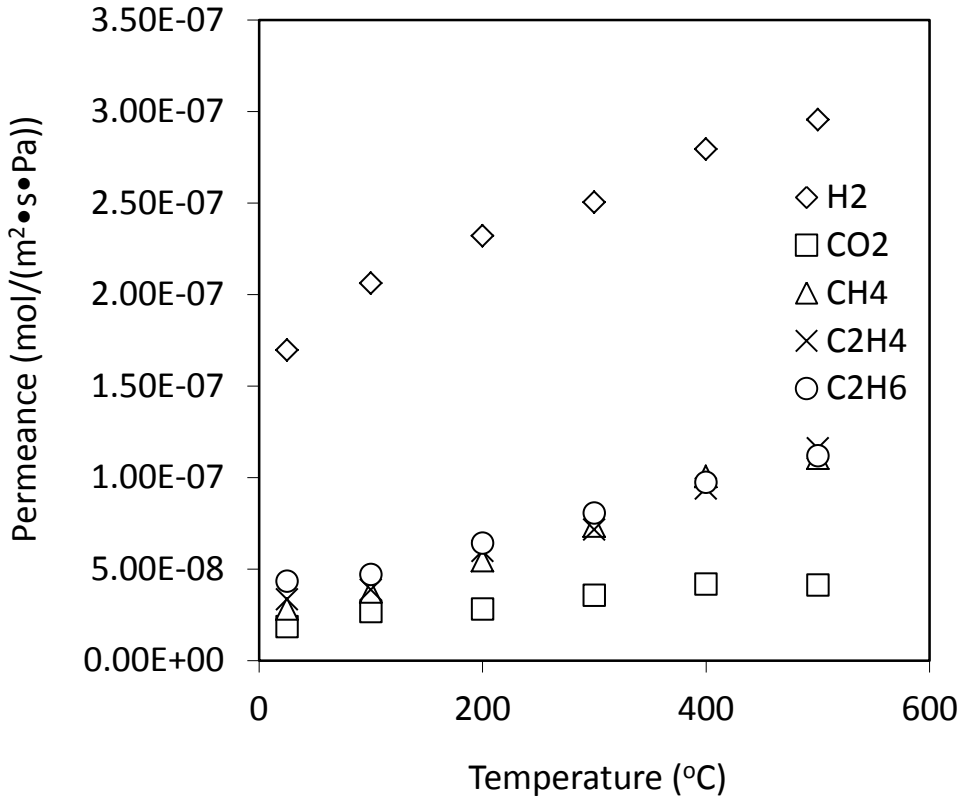

Figure 15. Gas permeance of H_2, CO_2, CH_4, C_2H_4, and C_2H_6 across a raw clinoptilolite membrane.

Knudsen separation selectivities of H_2 over CO_2, CH_4, C_2H_4 and C_2H_6 are 4.69, 2.83, 3.74, and 3.87, respectively. Selectivities of H_2 over CO_2, CH_4, C_2H_4, and C_2H_6 for the raw clinoptilolite membrane are presented in Figure 16. All selectivities remained above or close to their respective Knudsen values. Selectivities close to Knudsen are undesirable but they do indicate the absence of macroporous defects that allow free passage to all gas molecules. The results show that these high density deposits of natural clinoptilolite are promising as

membranes for H_2 separations and are good candidates for modification and upgrading to improve selectivities [15].

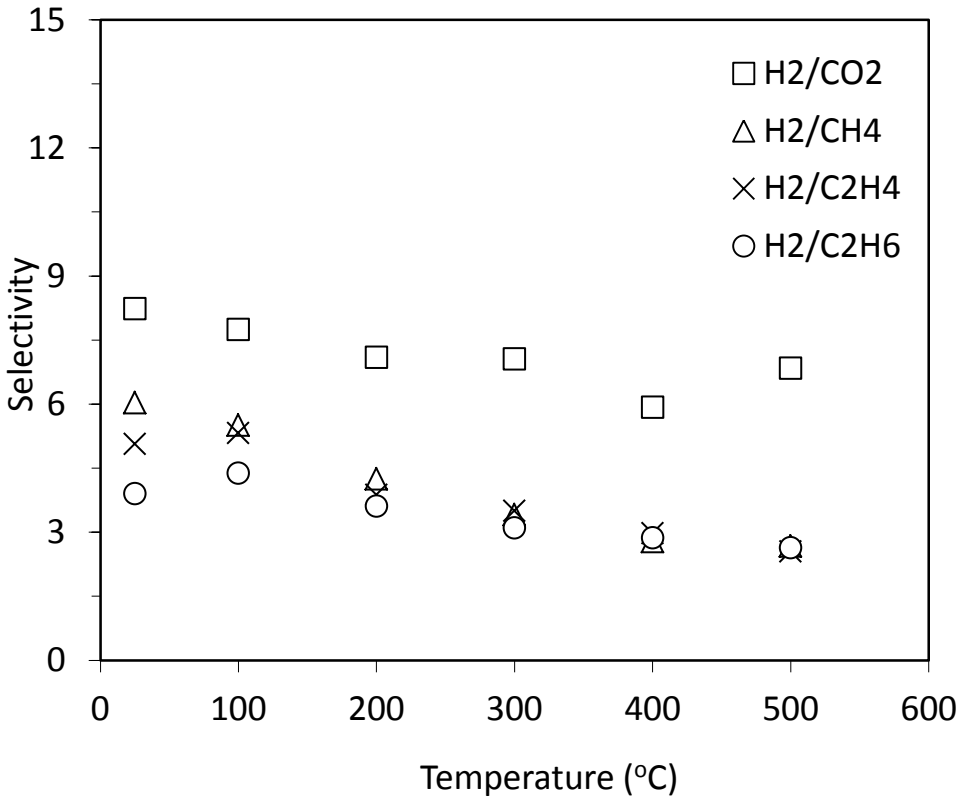

Figure 16. Selectivity of H_2 over CO_2, CH_4, C_2H_4, and C_2H_6 for a raw clinoptilolite membrane.

Permeation results for experiments performed using a surface-modified clinoptilolite membrane are presented in Figure 17. The permeance value for hydrogen at 25 ^{o}C remained essentially unchanged when compared to the

permeation results using raw clinoptilolite membranes (Figure 15). Permeance for carbon dioxide and the light hydrocarbons decreased significantly over the entire temperature range showing increased resistance to larger molecules crossing the membrane. For all gases the permeance became more temperature dependent after upgrading when compared to permeation results across the as-mined membrane. This behaviour is indicative of selective transport through the zeolite pores which implies that the surface modification is healing boundary defects.

Hydrogen permeance increased from approximately 2.7 x 10^{-7} mol/(m^2·s·Pa) to 5 x 10^{-7} mol/(m^2·s·Pa) as temperature increased from 25 ^{o}C to 500 ^{o}C [15]. The permeance values observed for the surface-modified membrane are comparable to permeance values found in other studies employing synthetic zeolite membranes [57-59]. This is particularly significant because the thickness of the zeolite layer in synthetic membranes is between 10-100µm while the thickness of the natural zeolite membranes in this study is approximately 1.2mm. This observation alone makes natural zeolites even more applicable as robust hydrogen selective membranes. Despite CH_4 having a larger molecular diameter than CO_2 its permeance was larger, indicating that separation isn't purely via size exclusion. It is presumed that differences in diffusivity and adsorption characteristics are also contributing [15].

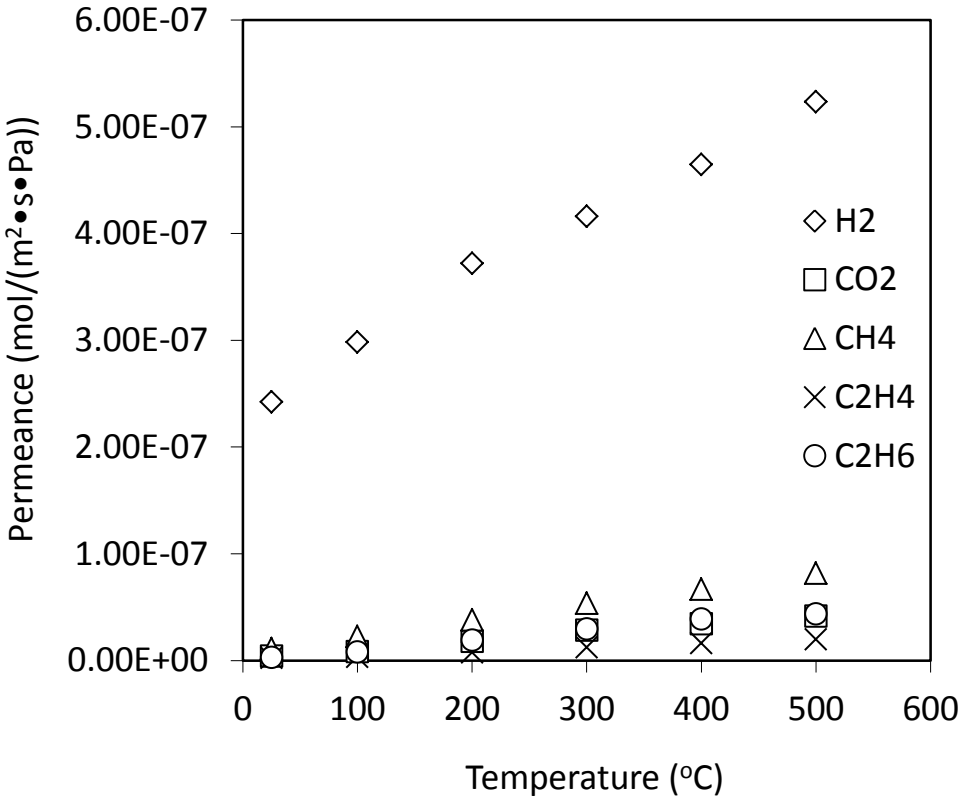

Figure 17. Gas permeances of H_2, CO_2, CH_4, C_2H_4, and C_2H_6 across a surface-modified clinoptilolite membrane.

The significant decrease in permeance for carbon dioxide and light hydrocarbons after surface-modification is followed by an increase in selectivities. Selectivities of H_2 over CO_2, CH_4, C_2H_4, and C_2H_6 for the surface-modified clinoptilolite membrane are presented in Figure 18. All selectivities remained well above Knudsen and in the case of H_2 over C_2H_4 a selectivity of nearly 100 was achieved at 25 ^oC. The selectivities of H_2 over CO_2, CH_4, C_2H_4, and C_2H_6 at 25 ^oC are 57.0, 22.0, 98.8, and 57.1, respectively. At higher

temperatures selectivities decrease but still remain above Knudsen. The selectivity of H_2 over CO_2, CH_4, C_2H_4, and C_2H_6 at 500 ^oC are 12.6, 6.4, 26.3, and 12.0, respectively. High selectivities and the temperature dependent permeances are a clear indication that the transport across the surface-modified membrane is occurring through zeolite pores and that an activated diffusion process is occurring [15].

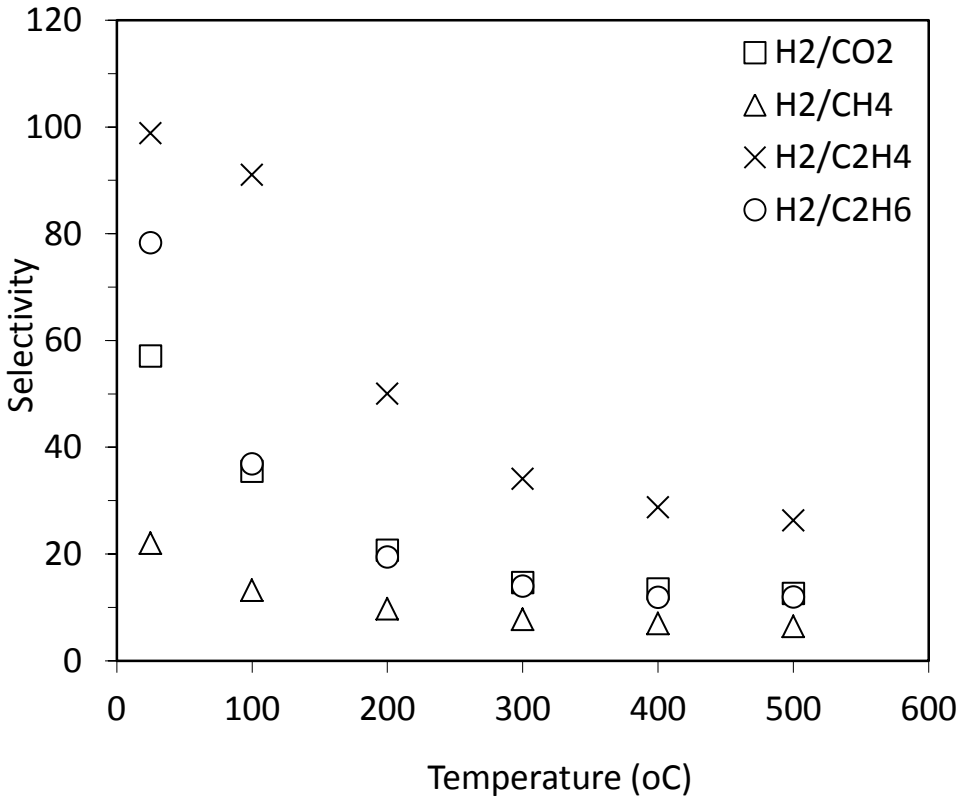

Figure 18. Selectivity of H_2 over CO_2, CH_4, C_2H_4, and C_2H_6 for a surface-modified clinoptilolite membrane.

3.1.3 Gas Membrane Thermal Stability

When using zeolites at the experimental temperature range being investigated, ensuring that the framework is not only stable but stable after several heating/cooling cycles is important. The hydrogen permeance for both raw and surface-modified membranes before and after several heating cycles is presented in Figure 19. In Figure 19(a) it can be seen that hydrogen permeance across the raw membrane decreases after several heating/cooling cycles. It was hypothesized earlier that there is potential phase transformation of impurities at higher temperatures which could be blocking zeolite pores. This could explain the decrease in hydrogen permeance shown in Figure 19(a). In Figure 19(b) it can be seen that hydrogen permeance across the surface-modified membrane is essentially unchanged after three heating/cooling cycles. As shown in the XRD and EDX analysis this increased stability is likely due to the surface-modification transforming or eliminating the less thermally stable impurities [15].

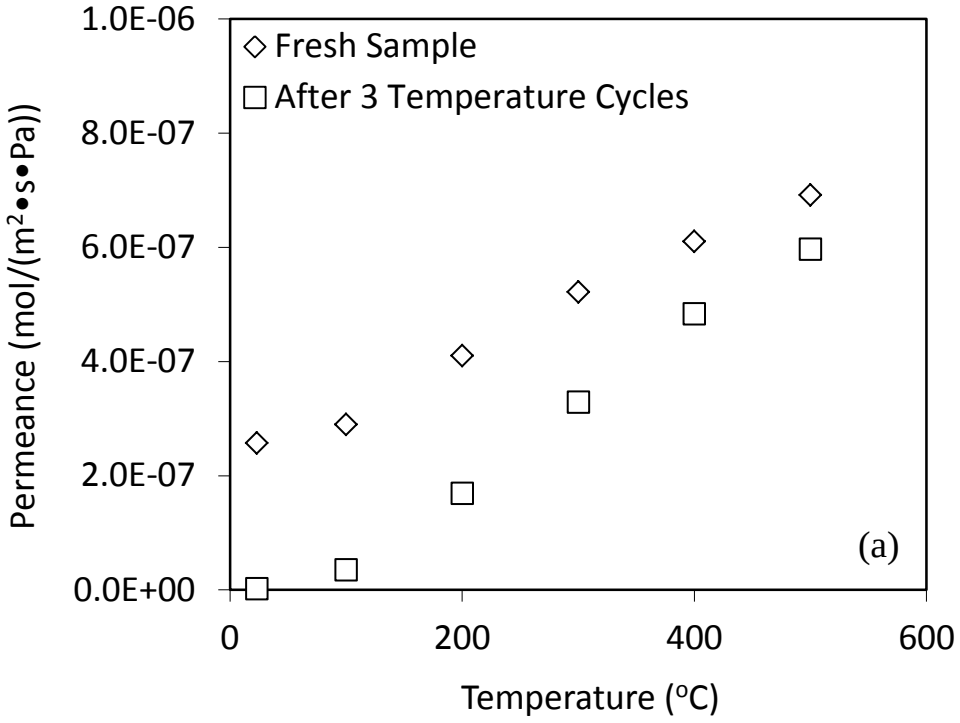

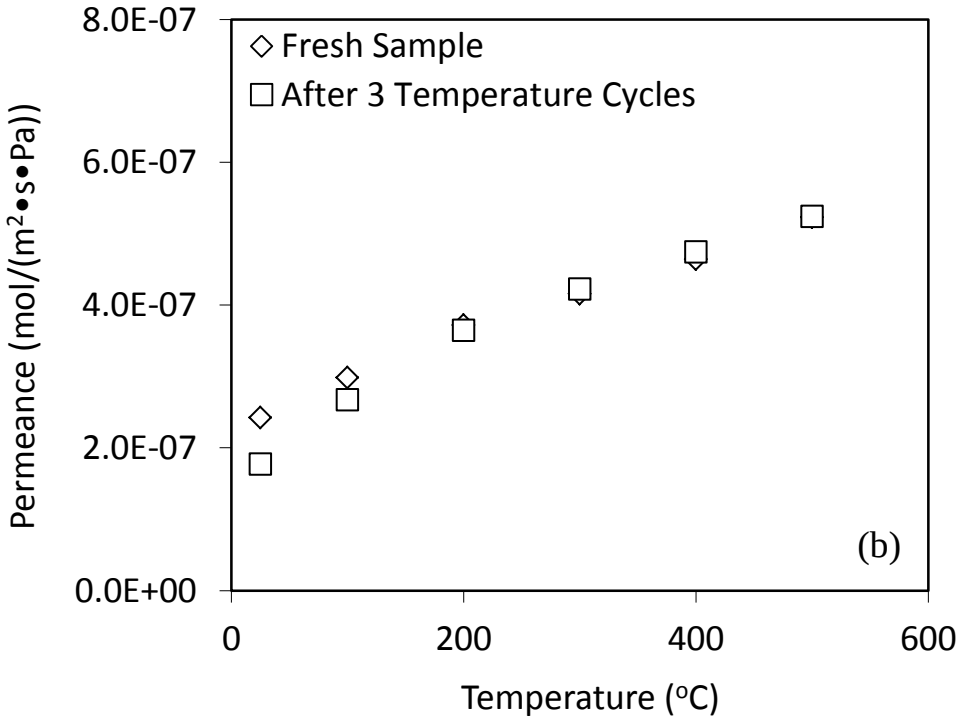

Figure 19. Hydrogen permeance before and after three heating/cooling cycles for (a) raw and (b) surface modified clinoptilolite membranes.

A unique deposit of high density clinoptilolite was identified from Castle Mountain, Australia with inherent characteristics suitable as a selective membrane for hydrogen separations. Proof of concept investigations using this material as membranes for separation of hydrogen from carbon dioxide and light hydrocarbons was conducted. As-mined, raw clinoptilolite membranes show selectivities above Knudsen, indicating that some of the transport across the membrane is through zeolitic pores. By a simple surface-modification pre-treatment the impurities with low thermal stabilities are either converted into a thermally stable phase or eliminated altogether. After surface modification, permeance of larger molecules decreases and selectivity of hydrogen over carbon dioxide and light hydrocarbons increases significantly. While further investigation into characterisation of the surface-modified membrane, identification of transport mechanism(s) and modelling and future scale-up is required, these preliminary results show great promise for the application of natural zeolites as hydrogen selective membranes.

3.2 Liquid Separations

3.2.1 Natural Zeolite Characterization

Scanning electron micrographs of the surface of the British Columbian natural zeolite are presented in Figure 20. The sample shown is the surface of a raw, unpolished, untested British Columbian natural zeolite. All samples were checked visually for fractures that may have propagated through the mineral

during excavation. Large fractures cause the membrane to break along the defect as soon as vacuum is applied to the permeate side. As can be seen in Figure 20, no fractures, defects or major impurities are present on the micron level. In porphyritic igneous rocks, such as the British Columbian zeolite sample, phenocrysts are a common occurrence. Phenocrysts are uniquely large crystals embedded in a finer crystal matrix and are typically not the same material as the fine crystal matrix. Both visual inspection and SEM images showed no phenocrysts in the British Columbia deposit [20]. The largest gap in the membrane surface is approximately 1 μm. Since in subsequent experiments high ion and organic rejections are observed it can be assumed that these gaps do not penetrate the entire thickness of the membrane. Presence of gaps in the uppermost layer of the natural zeolite membranes is not as detrimental as gaps in the surface layer of thin-film synthetic membranes which ruin the membrane [20].

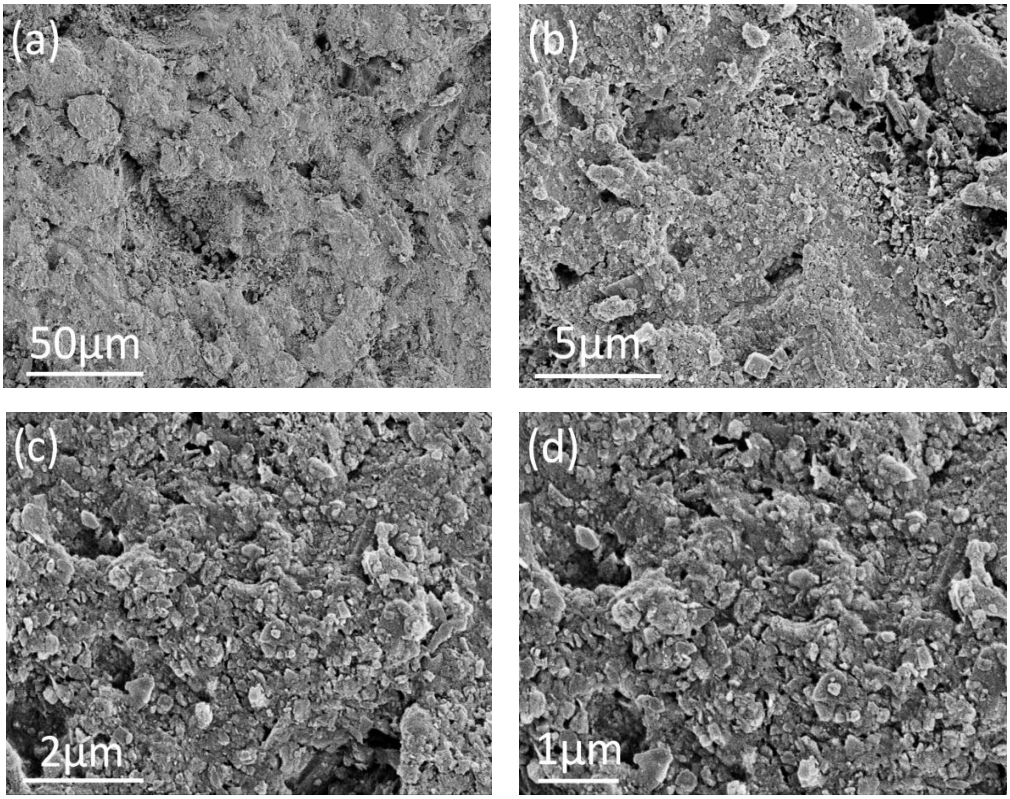

Figure 20. Scanning electron micrographs of raw, unpolished, untested British Columbian natural zeolite.

EDX elemental analysis was performed on the sample shown in Figure 20 and the results are presented in Table 3. Elemental variation between the two locations in the same deposit is apparent, which is consistent with natural zeolite materials. Sodium was not detected. It can be assumed that calcium and potassium are the dominant ions that balance the negatively charged framework. It is possible other cations that were not tested for are also present. By some definitions since more calcium than sodium is detected, this sample could be considered heulandite instead of clinoptilolite. But as discussed earlier

differentiating clinoptilolite and heulandite by cationic content is unreliable and doesn't provide enough insight into the zeolite properties. For this reason the Si/Al ratios for the two locations were calculated (Table 3) The Si/Al ratio for both locations is approximately 3.5. This correlates to the transition region of clinoptilolite and heulandite and could imply that throughout the mineral there are regions of both clinoptilolite and heulandites [20].

Table 3. EDX elemental analysis of raw, unpolished, untested British Columbian natural zeolite.

	Atomic Percent	
Element	Location 1	Location 2
Si	23.46	23.71
Al	6.95	7.21
Fe	1.75	1.19
Ca	2.7	2.82
Na	0	0
K	1.69	1.36
Cs	0	0
Ti	0.26	0.26
Mn	0.01	0
Si/Al	**3.51**	**3.42**

In order to confirm that both clinoptilolite and heulandite are present in the British Columbian deposit, XRD patterns of several different samples were analyzed. Two XRD patterns of raw, unpolished, untested samples from different locations in the deposit are shown in Figure 20. The HEU framework can be seen in both XRD patterns with Figure 20(a) being dominantly clinoptilolite and Figure 20(b) being dominantly heulandite. The characteristic peaks for the HEU framework have been indicated with stars. In both samples impurities are found, with the largest impurities being the feldspars albite and microcline. Although XRD alone is not a definite method to differentiate clinoptilolite and heulandite when coupled with the EDX results it strengthens the conclusion that both clinoptilolite and heulandite are present [20].

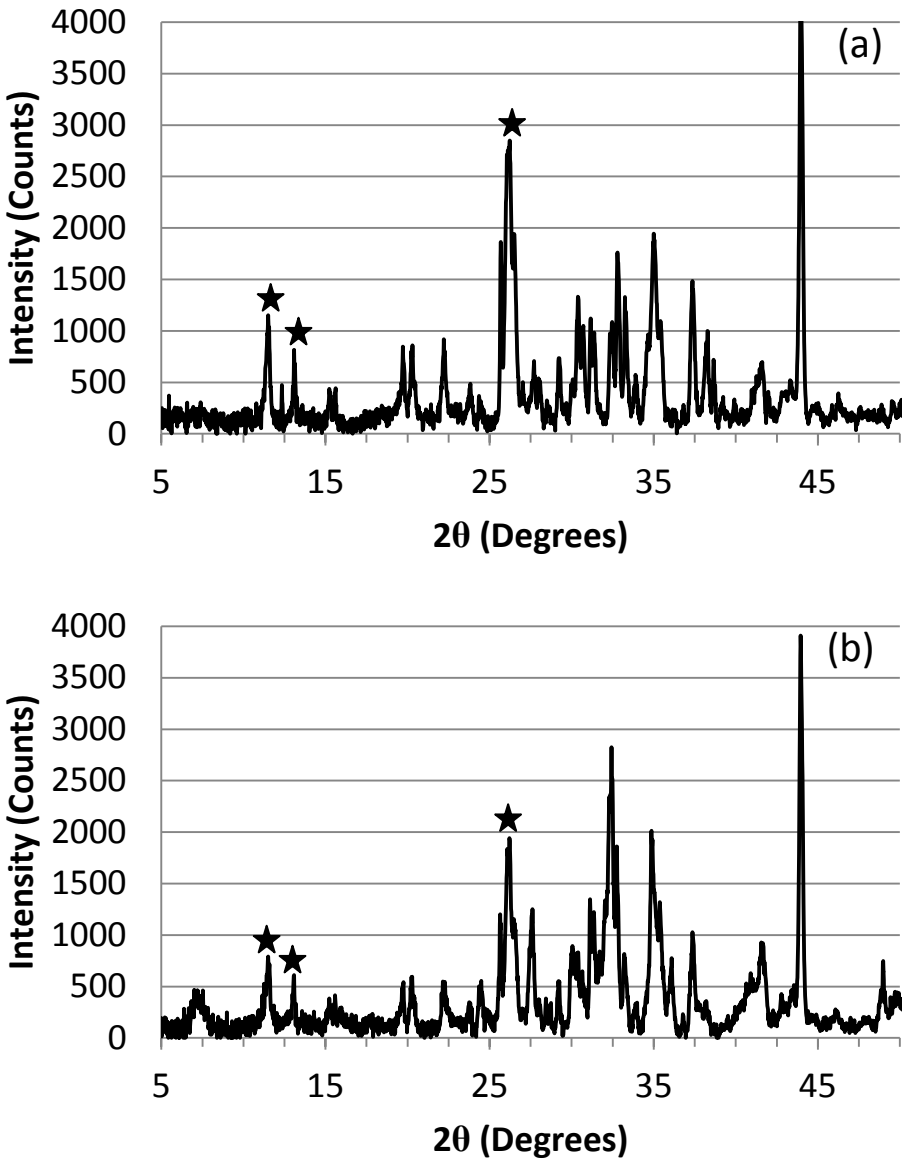

Figure 20. X-ray diffraction patterns for two raw, unpolished, untested British Columbian zeolite samples from two different locations in the deposit consisting of (a) dominantly clinoptilolite and (b) dominantly heulandite.

Nitrogen adsorption/desorption isotherms were performed on three different samples: raw, NH_4^+ exchanged calcined at 250 ^oC and NH_4^+ exchanged calcined at 450 ^oC. If the calcination temperature is sufficient the balancing cation in the zeolite will be hydrogen. But, if heulandite is the dominant mineral it is possible that the zeolite framework will collapse at higher calcination temperatures. This is because heulandite is not as thermally stable as clinoptilolite. To ensure that the framework remained intact after calcination, XRD patterns for all three samples were examined. These XRD patterns are presented in Figure 21 and the characteristic peaks of the HEU framework have been labelled with stars. If the peaks were to broaden that would indicate the framework is collapsing. At all three temperatures the HEU peaks remain strong, sharp, and at the same 2θ. Therefore, the HEU framework is not collapsing at 250 ^oC or 450 ^oC and remains intact.

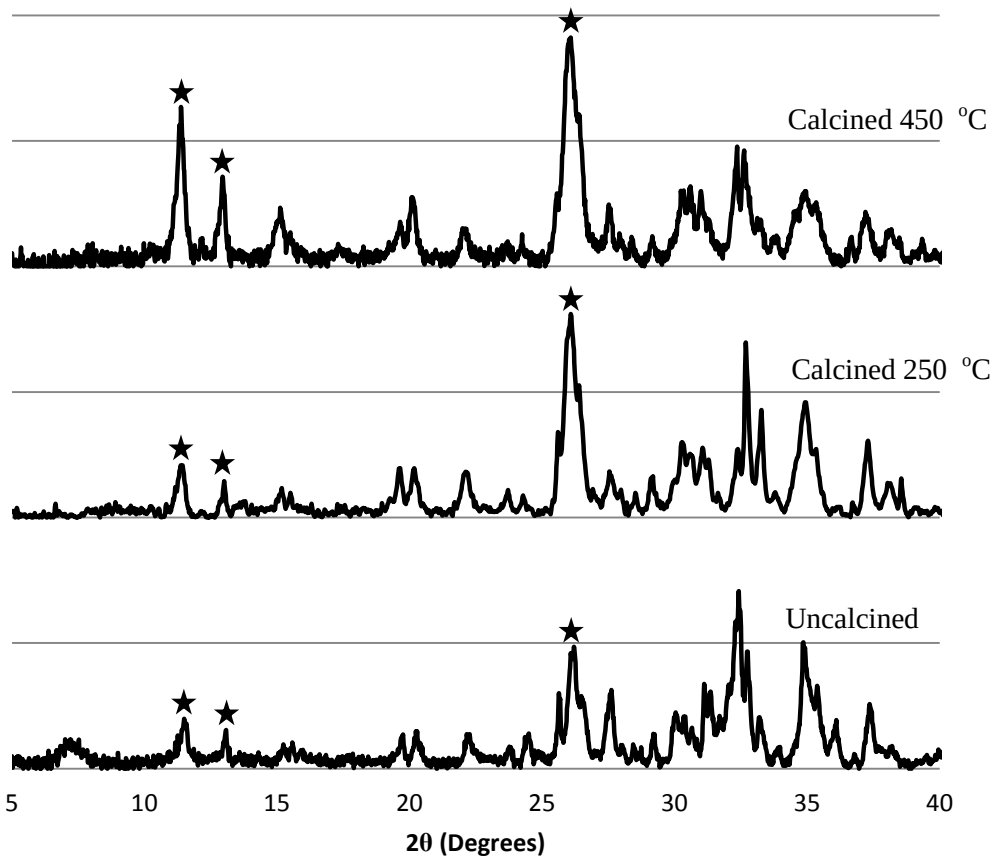

Figure 21. XRD patterns for the three samples used in BET surface area analysis.

Zeolite surface area can vary greatly and depends on purity, cationic content, Si/Al ratio and extra-framework water molecules. In naturally occurring microporous zeolites low surface areas are common because the larger cations in the pores do not permit nitrogen to enter all internal surfaces. The raw British Columbian zeolite was determined to have an external surface area of 13.98 m^2/g. Korkuna et al. studied the structural and physiochemical properties of a natural clinoptilolite deposit and found that their sample had an external surface area of

14.0 m^2/g [60]. Korkuna et al. reported clinoptilolite surface areas from other studies to be within the range of 11-27 m^2/g [60].

Nitrogen adsorption/desorption isotherms were used to determine the micropore volume. The micropore volume results are presented in Table 4. The British Columbian zeolite in its untreated form has no detectable micropore volume. This is because the larger cations detected in elemental analysis are blocking nitrogen from entering the 8 and 10 membered pore openings. When calcined at 250 ^oC the micropore volume increases very slightly. Therefore, the zeolite is not entirely in its hydrogen form and the balancing cation is still NH_4^+. The micropore volume increases substantially when calcined at 450 ^oC. The balancing cation is now hydrogen and the effective pore diameter is large enough for nitrogen to enter the pores. The effect of nitrogen only being able to enter the framework when the zeolite has been exchanged to the hydrogen form is common for the 8 and 10 member rings of micropores, and further supports the idea that this material is microporous and has the HEU framework.

Table 4. Micropore volume of natural British Columbian zeolite determined by nitrogen adsorption/desorption isotherms.

Calcination Temperature (^{o}C)	**Micropore Volume** (cc/g)
Raw Uncalcined Sample	0
250	0.00009649
450	0.03635

After a thorough characterization it can be concluded with confidence that natural zeolite samples from British Columbia constitute a high purity clinoptilolite/heulandite mineral with minimal macroporosity and minor impurities. Although heulandite has a lower thermal stability, for water permeation experiments this material is acceptable because the temperature required to destroy heulandite (<450 ^{o}C) is never reached. Therefore, this natural zeolite encompasses the desirable properties needed for a robust zeolite membrane for liquid separation applications [20].

3.2.2 Desalination Permeation Experiments

Desalination experiments were conducted and the membrane flux and the ion rejection at increasing salinities were monitored. The natural zeolite

membrane was exposed to increasing concentrations of Na^+ and a synthetic seawater. The results from pervaporation experiments using raw, unpolished membranes with water samples of varying salinity are shown Figure 22. All fluxes are averages of three runs at each temperature and salinity on the same membrane. Baseline water was initially tested to obtain fluxes over the entire temperature range and to determine the temperature dependence. When no additional salts were added the baseline flux is quite dependent on temperature. When temperature was increased from 25 ^oC to 93 ^oC baseline water flux increased from 0.4 $kg/m^2 \bullet h$ to 2.5 $kg/m^2 \bullet h$. When sodium chloride or sea salts were added both the temperature dependence and flux decreased [20]. The decrease in flux is more prominent at higher temperatures. The decrease in temperature dependence is demonstrated clearly in Figure 23. As sodium ion concentration increases the fluxes decrease and the range of fluxes at a given sodium ion concentration is much narrower.

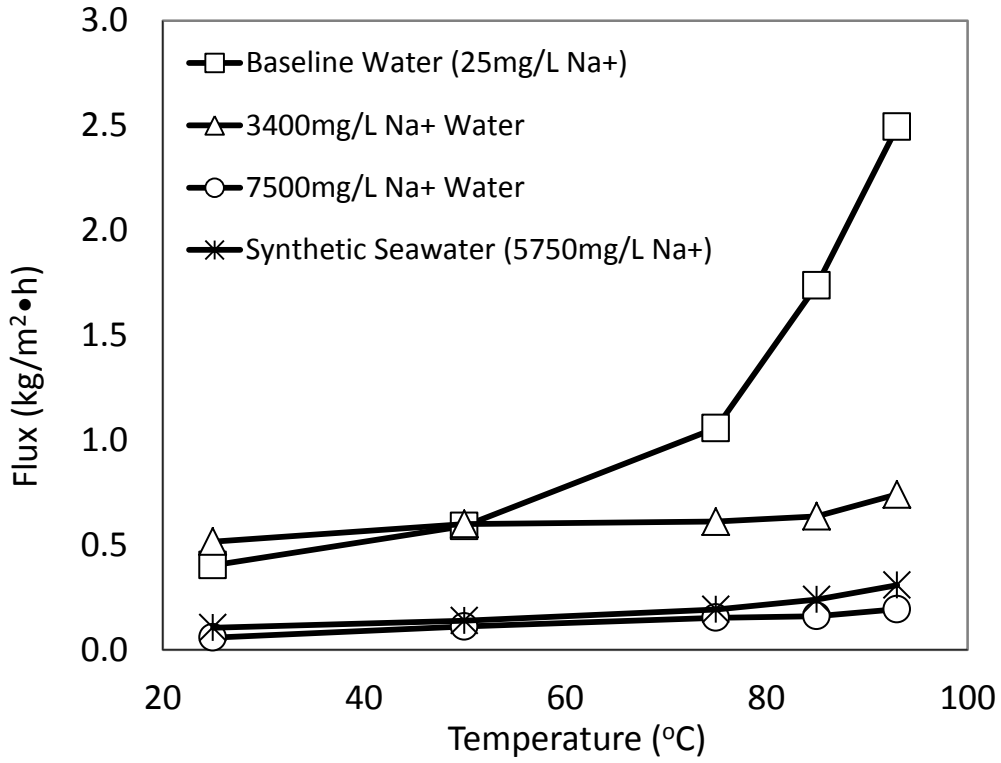

Figure 22. Pervaporation fluxes for British Columbian zeolite membranes exposed to increasing salinity of experimental water.

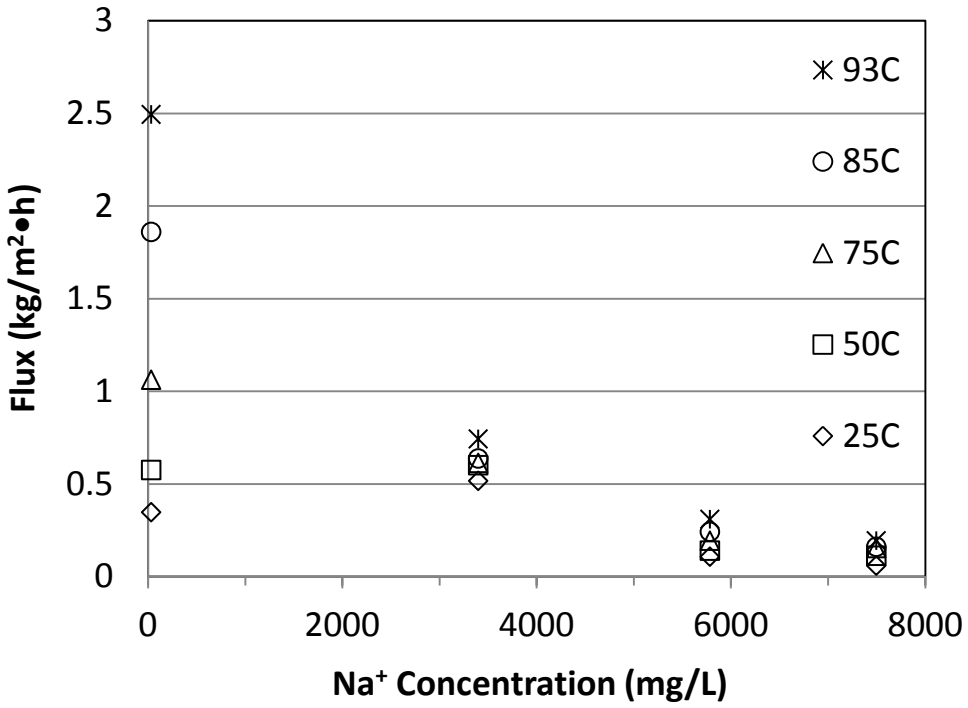

Figure 23. Pervaporation fluxes plotted against Na^+ concentration to illustrate decreasing temperature dependence and flux with increasing salinity.

The effect that the addition of salts has on zeolite membrane separations is subject to debate and is being investigated by several research groups [34,61]. The findings from different studies are not conclusive and in some cases contradictory. In our study it was found that as salt concentration increased flux dropped across the membrane [20]. Dotrement et al. performed pervaporation experiments separating chlorinated hydrocarbons from different concentrations of NaCl using a silicalite membrane [34]. It was observed that with increasing NaCl concentration there was a decrease in flux. The same effect was seen with the

addition of KCl, NaCl, Na_3PO_4, $FeCl_3$, and $CaCl_2$. This is in agreement with our work. One possible explanation to this increased resistance to mass transfer is the presence of concentration polarization. Another study employed a hydroxy sodalite membrane in the reverse osmosis desalination of seawater [61]. In this study the seawater had a higher flux than when pure water was tested. The authors concluded that even though further studies are needed, the presence of certain ions or counter ions could facilitate water transport across the membrane. This observation is the opposite of what was found in our study. Both studies show that even though further investigation is required to determine the exact mechanism(s) at work, salinity and counter ions can affect flux differently.

It is unlikely that the thermal/hydrothermal conditions or salinity in the pervaporation experiments would alter the zeolite framework but for thoroughness the XRD patterns of a membrane before testing and after exposure to synthetic seawater at all temperatures is shown in Figure 24. The XRD pattern shown after testing is of the feed side. As predicted there are no significant changes to the clinoptilolite/heulandite framework after the pervaporation experiments. Because high salinities are being tested it is possible that some scale, such as calcium carbonate, could have formed on the surface. No additional impurities or scale formation were found deposited on the membrane surface after it had been exposed to synthetic seawater at all temperatures [20].

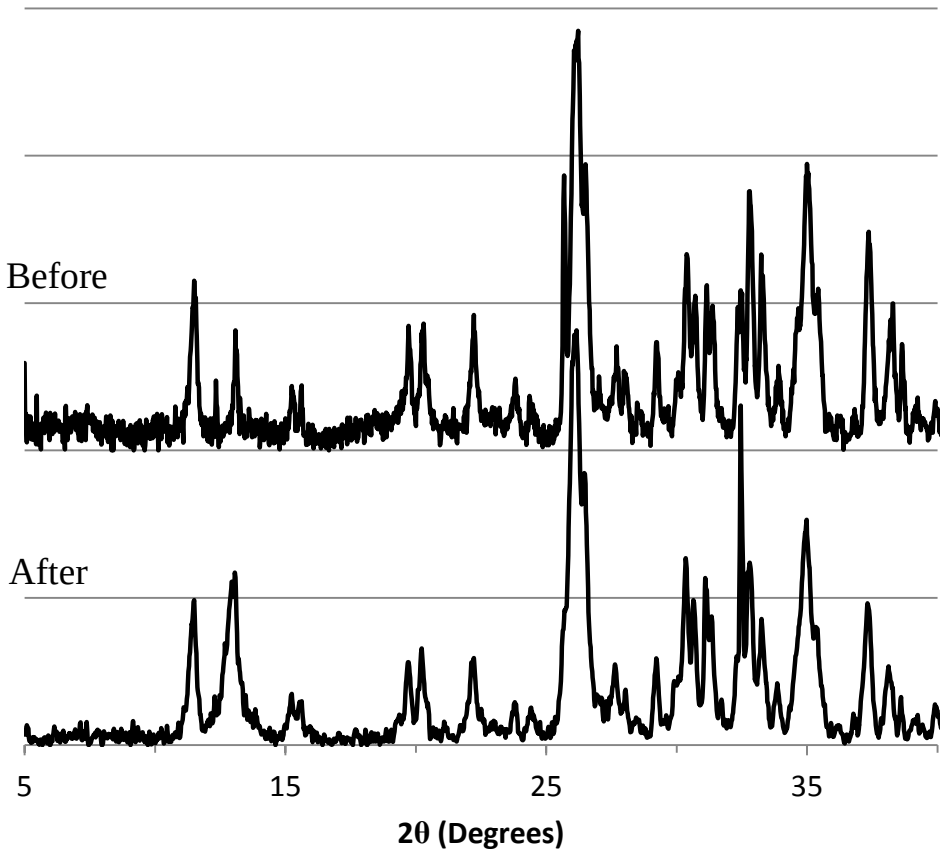

Figure 24. X-ray diffraction pattern for the feedside of the natural zeolite membrane before and after exposure to synthetic seawater at all temperatures.

Before continuing with the atomic absorption analysis from the pervaporation experiments a brief discussion of effective and hydrated radii of cations in water solutions is necessary. Since there is little macroporosity and few intercrystalline voids it can be inferred that a molecular sieving effect occurs and transport across the membrane happens dominantly through the clinoptilolite/heulandite pores. In solution cations are surrounded by a shell of

water molecules forming a hydration layer. This layer of water molecules creates a hydrated radius that is larger than the radius of the cation alone. The radius of the hydrated cation and the strength of hydration depend on factors such as concentration and ionic structure. Several research groups have focused on estimating cations' hydrated radius, the strength of hydration, and how many hydration layers are formed [62-65]. A literature summary of the effective and hydrated radii for Na^{+}, K^{+}, Ca^{2+}, and Mg^{2+} is presented in Table 5. The radius of cations in water has been the subject of extensive research but the determined hydrated radii varies between studies. An average was taken from several sources for the effective and hydrated radii of the various ions. In all cases, the average hydrated radii of the cations increased significantly from their average effective radii. The effective ionic radii follows this trend: $K^{+}>Ca^{2+}>Na^{+}>Mg^{2+}$, while the trend observed for the hydrated ionic radii is: $Mg^{2+}>Ca^{2+}>Na^{+}>K^{+}$. Knowing the increase in size of the hydrated cations is very important in this study, especially with synthetic seawater, to gauge the effectiveness of the natural zeolite membranes.

Table 5. Literature values for effective and hydrated radii for several cations.

	Effective Radius (Å)		**Hydrated Radius (Å)**	
	Value	**Ref.**	**Value**	**Ref.**
Na^+	1.011	[62]	1.78	[63]
	1.02	[63]	3.58	[64]
	1.17	[64]	2.99	[65]
	0.99	[65]		
Average	1.05		2.78	
K^+	1.377	[62]	2.01	[63]
	1.38	[63]	3.31	[64]
	1.49	[64]	2.75	[65]
	1.48	[65]		
Average	1.43		2.69	
Ca^{2+}	1.005	[62]	3	[63]
	1.23	[63]	4.12	[64]
	1	[64]		
Average	1.08		3.56	
Mg^{2+}	0.72	[62]	3	[63]
	0.72	[63]	4.28	[64]
	0.72	[64]		
Average	0.72		3.64	

Despite the noted decrease in flux when testing synthetic seawater ion rejections remained high. In Figure 25 the atomic absorption results for Na+ rejection across the entire temperature range tested are shown. Na^+ rejections at 27 ^oC, 50 ^oC, 75 ^oC, 85 ^oC and 93 ^oC are 99.7%, 98.8%, 98.7%, 99.3%, and 95.8%, respectively. As temperature increases Na^+ rejection drops slightly but still remains greater than 95%. For pervaporation experiments done with synthetic seawater, along with Na^+ rejection, Ca^{2+}, Mg^{2+} and K^+ rejections were also analyzed. The atomic absorption results for Na^+, Ca^{2+}, Mg^{2+} and K^+ at 75 ^oC are presented in Figure 26. The hydrated radii have also been added to the bottom of Figure 26. Ion rejections at 75 ^oC for Na^+, Ca^{2+}, Mg^{2+} and K^+ are 98.7%, 98.5%, 99.9%, and 98.4%, respectively. The absence of calcium and magnesium ions in the permeate, coupled with trace presence of sodium and potassium, can be explained by molecular sieving of the ions in their hydrated forms. For all the salinities tested the percent rejection for the tested cations increases in the same order as their hydrated radii [20].

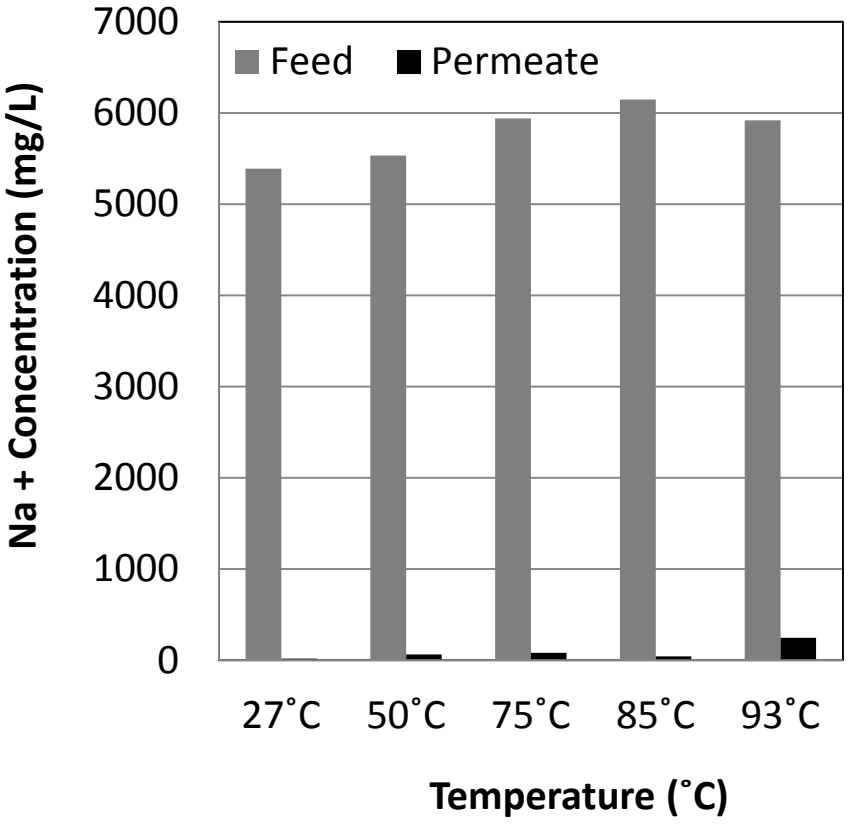

Figure 25. Sodium ion concentrations in the feed and permeate at 27 ^{o}C to 93 ^{o}C from pervaporative desalination of synthetic seawater using a natural zeolite membrane.

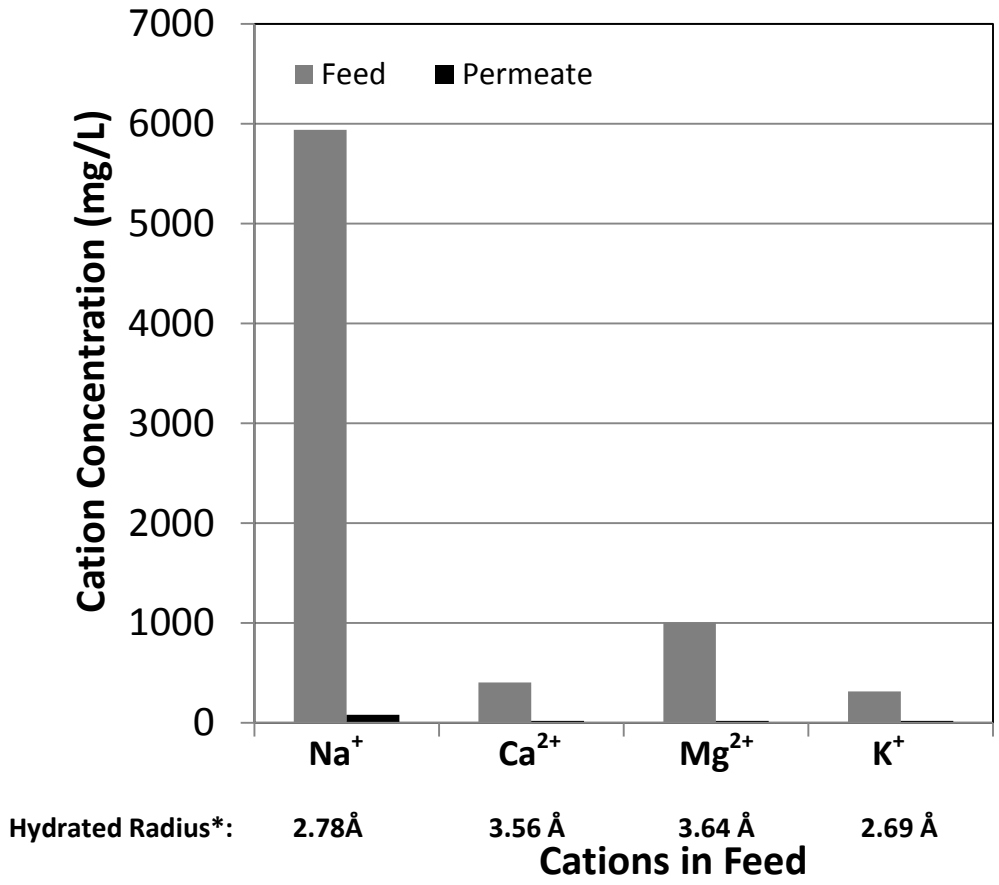

Figure 26. Ion concentrations in feed and permeate at 75 ^{o}C pervaporative desalination of synthetic seawater using a natural zeolite membrane.

Although many studies have investigated the use of synthetic zeolites in membrane applications few studies to date have considered natural zeolites. In this study high density, high purity clinoptilolite/heulandite minerals were machined into thin sections and were employed as novel, robust, hydrothermally stable desalination membranes. For the desalination industry, these natural zeolite membranes could represent a viable alternative to thin-film membranes. The

natural zeolite membranes tested effectively desalinated a synthetic seawater while the clinoptilolite/heulandite framework remained intact and free of scale after exposure to high temperatures and high salinities. Although further studies are required to understand the lack of temperature dependency at high salinities and to improve the flux natural zeolite membranes show promise in desalination applications.

3.2.3 Organic Separation Experiments

An XRD pattern for a different sample of British Columbia natural zeolite (but the same deposit as the sample used for desalination experiments) is shown in Figure 27. The characteristic peaks of the HEU framework have been marked with stars. The results are consistent with the results from the sample used for the desalination experiments. Since the XRD patterns between samples from the same deposit are so similar no further characterisation was done for membranes prepared for organic separation experiments.

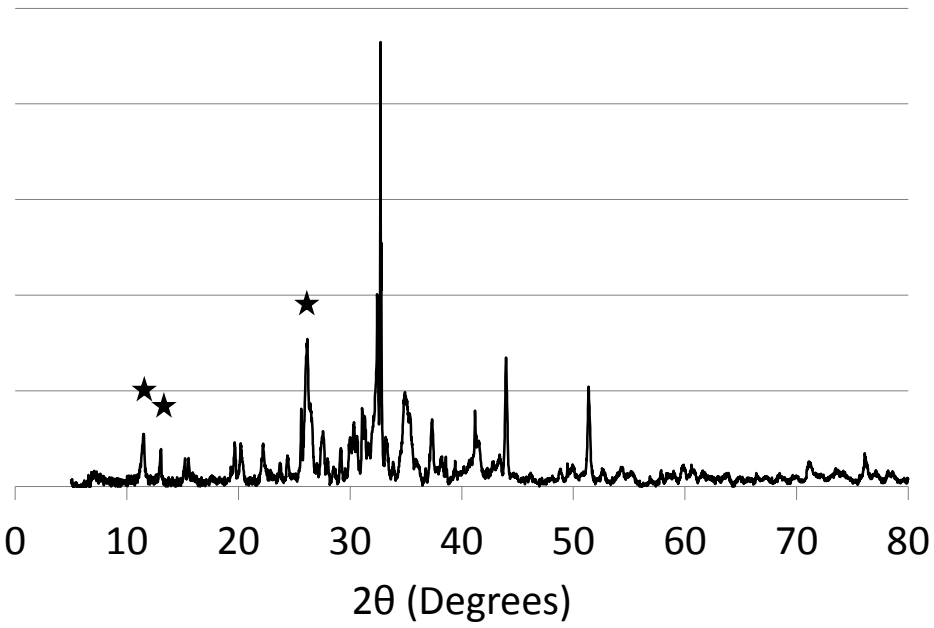

Figure 27. XRD pattern of a different sample of clinoptilolite/heulandite from the British Columbia deposit.

The ionic content of the synthetic process water prepared for these experiments was determined by averaging the ionic concentrations from several actual produced water samples. In Table 6 the ionic concentrations for several actual produced water samples and the synthetic process water used in this study are presented. The concentration of Na^+ for the actual produced water samples was always the highest so it was used to determine how much Sea Salt was needed for making the synthetic seawater. The consequence of this was that the concentrations of Ca^{2+}, Mg^{2+} and K^+ are higher than those found in the actual produced water samples. Since there is a large amount of variability in the salts

present in oil sands deposits the synthesized ionic mixture can serve as a synthetic process water.

Table 6. Ionic concentrations of several actual process water samples and the synthetic process water used in this study.

	Concentration in Process Water (mg/L)					
Cations	[56]	[56]	[53]	[53]	[14]	Synthetic Process Water
Sodium, Na^+	2200	780	706	1616	1420	1159
Calcium, Ca^{2+}	3	22	4	23	8	93
Magnesium, Mg^{2+}	6	11	0	13	0	169
Potassium, K^+	62	13	28.7	68	30	289

In the desalination experiments, as mentioned earlier, increasing salinity decreased the flux across the entire temperature range especially at higher temperatures. When toluene concentration was increased the flux decreased slightly but did not have as significant an impact as increasing salinity. The results from pervaporation experiments conducted at 85 ^oC with increasing toluene concentration are presented in Figure 28. When no toluene was added the flux

with its 95% confidence interval was 0.53±0.10 kg/m^{2}hr (this is the average of seven runs on the same membrane). For toluene concentrations below 60 mg/L the fluxes are within the 95% confidence interval of the flux when no toluene was added. Therefore, at low concentrations the slight decrease in flux is not statistically significant. But, at toluene concentrations higher than 100 mg/L there is a larger decrease in fluxes that no longer lie within the 95% confidence interval of the flux when no toluene was added. Due to the low solubility of toluene, higher concentrations of toluene in the synthetic process water could not be achieved at 85 ^{o}C. However, it is clear from the toluene concentration range tested that the effect of toluene addition is not as significant as increasing salinity.

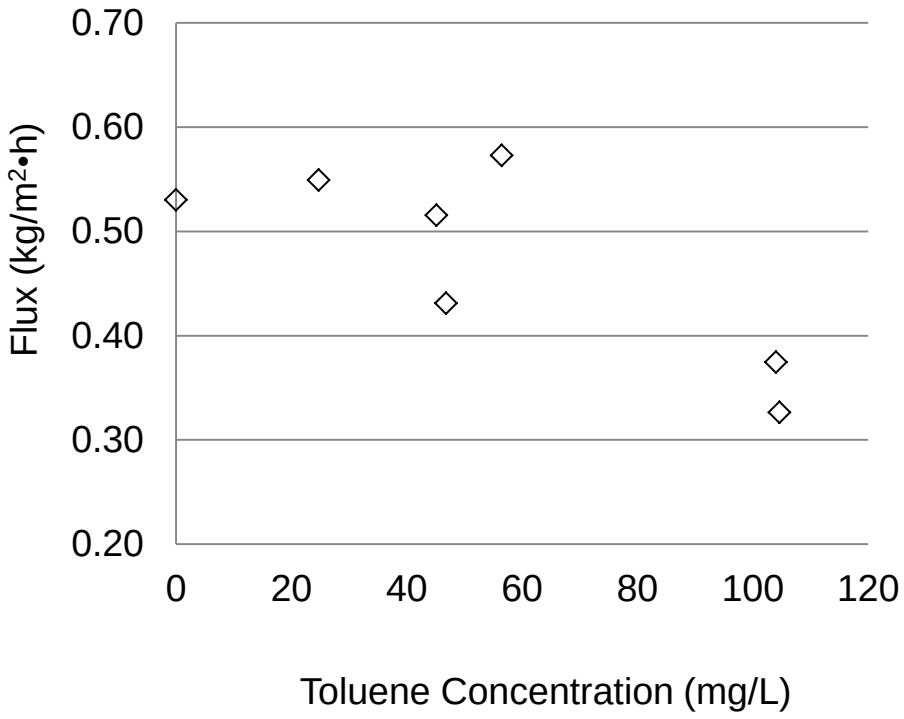

Figure 28. Pervaporation experiment results at 85 ^{o}C with increasing toluene concentration.

The atomic absorption results from the pervaporation experiments at 85 ^{o}C using a synthetic process water are presented in Table 7. Na^{+} concentrations were reduced by 87% and cations with larger hydrated radii showed rejections greater than 99%. Since Ca^{2+} has a hydrated radius close to that of Mg^{2+} an equally high rejection for Ca^{2+} can be inferred.

Table 7. Atomic absorption results from pervaporation experiments done at 85 ^{o}C using a synthetic process water.

	Temperature (^{o}C)	Amount (mg/L)		
		Na^{+}	Mg^{++}	K^{+}
Synthetic Process Water	-	1158.9	169.6	289.8
Concentration in Permeate	85	146.2	0.2	1.8
% Rejection	-	87.4	99.9	99.4

As shown in Figure 28, the toluene concentrations in the synthetic seawater at 85 ^{o}C ranged from approximately 25 mg/L to 100 mg/L. No toluene was detectable by GC-FID in the permeate stream for all concentrations of toluene tested at 85 ^{o}C. For the GC-FID used in this study the lowest detection limit for toluene was approximately 1 mg/L. Although rejection could possibly be higher the only supported conclusion is that toluene concentrations were decreased to 1 mg/L for all tested concentrations. This translates to toluene rejections of greater than 96% and 99% for feed toluene concentrations of 25 mg/L and 100 mg/L, respectively. Investigations of higher concentrations could be conducted by either hermetically sealing the synthetic process water vessel or by analyzing a more soluble model organic compound. Future studies with model

organics with different functionality, such as model naphthenic acids, should also be considered.

Chapter 4. Conclusions

Unique, high density deposits of the natural zeolite clinoptilolite have been identified, characterized and experimentally applied as novel, robust membranes for hydrogen separation and water purification. The results of this study show that natural zeolite membranes have great potential as chemically and thermally stable, economical alternatives to their synthetic thin-film counterparts.

As-mined Castle Mountain clinoptilolite gas separation membranes showed relatively stable permeances with hydrogen selectivities up to nearly twice Knudsen selectivity, indicating zeolitic contribution to overall permeation. With a simple surface-modification pre-treatment impurities with lower thermal stability were either recrystallized into a more stable phase or removed altogether. This pre-treatment greatly decreased permeance of carbon dioxide and light hydrocarbons by healing the intercrystalline voids and boundary defects which allowed transport to larger molecules across as-mined membranes. Selectivities for hydrogen over carbon dioxide and light hydrocarbon rose significantly after surface-modification far surpassing selectivity predicted by Knudsen diffusion. Raw membranes showed a decrease in hydrogen permeance after several heating/cooling cycles, while pre-treated membranes exhibited very stable hydrogen permeances indicating high thermal stability. These proof of concept experiments clearly show that the natural zeolite membranes warrant further investigation and could become economically feasible for industrial application for hydrogen purification.

A second deposit of high density clinoptilolite was identified in British Columbia and was utilized for membrane water purification. The water purification processes investigated were desalination of a synthetic seawater and reclaiming process water. Thorough characterisation showed that the British Columbian zeolite is dominantly clinoptilolite/heulandite and has inherent properties suitable for application as a water purification membrane and for future modification and upgrading. Pervaporation studies employing a synthetic seawater showed efficient flux and high ion rejection over a wide range of temperatures. The zeolite framework remained intact after exposure to high temperatures and high salinities and no scale formation was detected. The ion rejections were found to show increasing rejections in the same order as their hydrated radii, not their effective radii. A synthetic process water was also tested investigating the potential application of the clinoptilolite/heulandite membranes as a once-through membrane process for reclaiming process waters. In these experiments the ion rejections remained high and essentially all toluene was removed. Despite there being much debate on the exact mechanism(s) that control transport and the effect of ionic concentration on synthetic zeolite membranes, natural zeolite membranes are beginning to become a reality for desalination and process water reclamation and not just a theoretical curiosity.

Zeolite molecular sieves form the backbone of countless industrial processes and are the focus of many research applications. While much research attention is being directed at the characterisation, development, modelling and eventually industrial application of synthetic thin-film zeolite membranes to date

few investigations into natural zeolite membranes have been conducted. In this study it was demonstrated that unique high density zeolite deposits can be applied as mechanically, thermally and chemically stable membranes for hydrogen separation, desalination and reclaiming process water.

Future Work

Further characterisation of the surface-modification of the gas separation membranes will aid in understanding the transport mechanisms contributing to overall permeation and variations to the current pre-treatment which may be more effective. By modifying the membrane surface high selectivities were achieved by lowering the permeances of carbon dioxide and light hydrocarbons but to increase selectivities further work should focus on increasing hydrogen permeance. By investigating different surface modifications perhaps the less thermally stable impurities could be recrystallized into another crystalline zeolite phase that could increase hydrogen permeance. All water membrane separations were performed using raw, as-mined British Columbian zeolite and higher fluxes could be achieved be applying a pre-treatment modification.

For gas and water separations the issue of scale-up will eventually need to be addressed. For natural zeolite membranes to find economical application there will need to be a shift away from sectioned membranes to where different membrane configurations, such as tubes, can be formed with ease. Incorporating

the powdered zeolite in a cement or polymer matrix could serve as the next step of experimentation.

While further investigation into characterisation of the surface-modified membrane, transport mechanism identification and modelling and future scale-up is required these preliminary results show great promise for the application of natural zeolites as hydrogen selective membranes.

Chapter 5. Bibliography

[1] M. Kazemimoghadam, T. Mohammadi. Synthesis of MFI zeolite membranes for water desalination. Desalination, 206 (2007) 547.

[2] A. Anson, S.M. Kuznicki, T. Kuznicki, B.G. Dunn, E.M. Eyring, and D.B. Hunter. Separation of argon and oxygen by adsorption on a titanosilicate molecular sieve. Separation Science and Technology, 44 (2009) 1604.

[3] A. Anson, S.M. Kuznicki, T. Kuznicki, T. Haastrup, Y. Wang, C.C.H. Lin, J.A. Sawada, E.M. Eyring, and D. Hunter. Adsorption of argon, oxygen, and nitrogen on silver exchanged ETS-10 molecular sieve. Microporous and Mesoporous Materials, 109 (2008) 577.

[4] G. Tonetto, J. Atias, and H. de Lasa. FCC catalysts with different zeolite crystallite sizes: acidity, structural properties and reactivity. Applied Catalysis A: General, 270 (2004) 9.

[5] G. Gottardi, E. Gallim, Natural Zeolites, Germany, Springer-Verlag Berlin Heidelberg, 1985.

[6] D.W. Breck, Zeolite Molecular Sieves, New York, Wiley—Interscience, 1974.

[7] D.L. Bish, D.W. Ming, Natural Zeolites: Occurrence, Properties, Application, Reviews in Mineraloogy & Geochemistry, 45 (2001).

[8] F.A. Mumpton, Mineralogy and Geology of Natural Zeolites, (1977) 233.

[9] J. Lin, I. Kumakiri, B. Nair, and H. Alsyouri. Microporous Inorganic Membranes. Separation & Purification Methods, 31 (2002) 229.

[10] A.S.M. Junaid, H. Yin, A. Koenig, P. Swenson, J. Chowdhury, G. Burland, W.C. McCaffrey and S.M Kuznicki. Natural zeolite catalyzed cracking-assisted light hydrocarbon extraction of bitumen from Athabasca oilsands. Applied Catalysis A: General, 354 (2009) 44.

[11] A.S.M. Junaid, M. Rahman, H. Yin, W.C. McCaffrey, and S.M. Kuznicki. Natural zeolites for oilsands bitumen cracking: Structure and acidity. (2011).

[12] A.S.M. Junaid, W. Wang, C. Street, M. Rahman, M. Gersbach, S. Zhou, W.C. McCaffrey, and S.M. Kuznicki. Viscosity reduction and upgrading of athabasca oilsands bitumen by natural zeolite cracking. Proceedings of World Academy of Science, Engineering and Technology, 69 (2010) 695.

[13] W.T. Schaller. The mordenite-ptilolite group; clinoptilolite a new species. American Mineralogist, 17 (1932) 128.

[14] M. Bridle. Treatment of SAGD Produced Waters Without Lime Softenning. Society of Petroleum Engineers, (2005).

[15] W. An, P. Swenson, L. Wu, T. Waller, A. Ku, and S.M. Kuznicki. Selective separation of hydrogen from C1/C2 hydrocarbons and CO2 through dense natural zeolite membranes. Journal of Membrane Science, 369 (2011) 414.

[16] D. Zhao, K. Cleare, C. Oliver, C. Ingram, D. Cook, R. Szostak, and L. Kevan. Characteristics of the synthetic heulandite-clinoptilolite family of zeolites. Microporous and Mesoporous Materials, 21 (1998) 371.

[17] S. Satokawa, K. Itabashi. Crystallization of single phase (K, Na)-clinoptilolite. Microporous Materials, 8 (1997) 49.

[18] R. Gao, H.P. van Leeuwen, H.J.F. van Valenberg, and M.A.J.S. van Boekel. Accurate determination of the Ca2+ activity in milk-based systems by Ca-ISE: Effects of ionic composition on the single Ca2+ activity coefficient and liquid junction potentials. Food Chemistry, 129 (2011) 619.

[19] C. Baerlocher, L.B. McCusker, Database of Zeolite Structures, IZA, (2011).

[20] P. Swenson, B. Tanchuk, A. Gupta, W. An, and S.M. Kuznicki, Pervaporative Desalination of Water Using Natural Zeolite Membranes, (2011).

[21] T. Matsuura, Synthetic Membranes and Membrane Separation Processes, Boca Raton, Florida, CRC Press, 1994.

[22] K.W. Böddeker, Liquid Separations with Membranes: An Introduction to Barrier Interference, Springer.

[23] K.W. Böddeker. Commentary: Tracing membrane science. Journal of Membrane Science, 100 (1995) 65.

[24] S.P. Nunes, K. Peinemann, Membrane Technology in the Chemical Industry, Wiley (2006).

[25] J. Caro, M. Noack, Zeolite membranes - from Barrers vision to technical applications: new concepts in zeolite membrane R&D, in Ruren Xu, Zi Gao,Jiesheng Chen and Wenfu Yan (Ed.), Studies in Surface Science and Catalysis, Elsevier, 2007, pp. 96-109.

[26] J. Romero, C. Gijiu, J. Sanchez, and G.M. Rios. A unified approach of gas, liquid and supercritical solvent transport through microporous membranes. Chemical Engineering Science, 59 (2004) 1569.

[27] H. Ahn, D. Jeong, H. Jeong, and Y. Lee. Pervaporation characteristics of trichlorinated organic compounds through Silicalite-1 zeolite membrane. Desalination, 245 (2009) 754.

[28] K.P. Lee, T.C. Arnot, and D. Mattia. A review of reverse osmosis membrane materials for desalination - Development to date and future potential. Journal of Membrane Science, 370 (2011) 1.

[29] A. Julbe, Chapter 6 Zeolite membranes — synthesis, characterization and application, Studies in Surface Science and Catalysis, Elsevier, 2007, pp. 181-219.

[30] M.C. Duke, J. O`Briend-Abraha, N. Milne, B. Zhu, J.Y.S. Lin, and J.C.D. Costa. Seawater desalination performance of MFI type membranes made by secondary growth. Separation and Purification Technology, 68 (2009) 343.

[31] S.D. Seader, E.J. Henley, Separation Process Principles, John Wiley & Sons, 2006.

[32] R. Krishna. A unified approach to the modelling of intraparticle diffusion in adsorption processes. Gas Separation & Purification, 7 (1993) 91.

[33] D.M. Ruthven, Principles of Adsorption and Adsorption Processes, New York, John Wiley, 1984.

[34] C. Dotrement, S. Van der Ende, H. Vandemmele, and C. Vandecsteele. Concentration Polarization and other Boundary Layyer Effects in the Pervaporation of Chlorinated Hydrocarbons. Desalination, (1994) 91.

[35] D.A. Ladner, A. Subramani, M. Kumar, S.S. Adham, and M.M. Clark. Bench-scale evaluation of seawater desalination by reverse osmosis. Desalination, 250 (2010) 490.

[36] R.A.D. Rand, R.M. Dell, Hydrogen Energy Challenges and Prospects, Cambridge, UK, RSC Publishing, 2008.

[37] K. Liu, C. Song, and V. Subramani, Hydrogen and Syngas Production and Purification Technologies, Hoboken, NJ, USA, Wiley, 2009.

[38] R.H. Jones, G.J. Thomas, Materials for the Hydrogen Economy, Boca Raton, Fl, CRC Press, 2008.

[39] J.A. Ritter, A.D. Ebner. State-of-the-Art Adsorption and Membrane Separation Processes for Hydrogen Production in the Chemical and Petrochemical Industries. Separation Science & Technology, 42 (2007) 1123.

[40] GEO-Global Environment Outlook 3, Past, Present and Future Perspective, Earthscan Publications Ltd, Sterling, VA 2002.

[41] K. Madwar, and H. Tarazi. Desalination techniques for industrial wastewater reuse. Desalination, 152 (2003) 325.

[42] S.S. Mitra, A.R. Thomas, and G.T. Gang. Evaluation and characterization of seawater RO membrane fouling. Desalination, 247 (2009) 94.

[43] J. Mallevialle, P.E. Odendall, and M.R. Wiesner, Water Treatment Membrane Processes, McGraw-Hill (1996).

[44] T.C. Bowen, R.D. Noble, and J.L. Falconer. Fundamentals and applications of pervaporation through zeolite membranes. Journal of Membrane Science, 245 (2004) 1.

[45] S. Wee, C.T. Tye, and S. Bhatia. Membrane separation process - Pervaporation through zeolite membrane. Separation and Purification Technology, 63 (2008) 500.

[46] Q. Liu, R.D. Noble, J.L. Falconer, and H.H. Funke. Organics/water separation by pervaporation with a zeolite membrane. Journal of Membrane Science, 117 (1996) 163.

[47] X. Chen, X. Lin, P. Chen, and H. Kita. Pervaporation of ketone/water mixtures through silicalite membrane. Desalination, 234 (2008) 286.

[48] J. Lin, S. Murad. A computer simulation study of the separation of acqueous solutions using thin zeolite membranes. Molecular Physics, 99 (2001) 1175.

[49] C.H. Cho, K.Y. Oh, S.K. Kim, J.G. Yeo, and P. Sharma. Pervaporative seawater desalination using NaA zeolite membrane: Mechanisms of high water flux and high salt rejection. Journal of Membrane Science, 371 (2011) 226.

[50] S. Khajavi, J.C. Jansen, and F. Kapteijn. Production of ultra pure water by desalination of seawater using hydroxy sodalite membrane. Journal of Membrane Science, 356 (2010) 52.

[51] Energy Resources Conservation Board, Alberta's Energy Reserves 2009 and Supply/Demand Outlook 2010-2019 2010.

[52] A.M. Albahlani, T. Babadagli. A Critical Review of the Status of SAGD: Where are we and what is next? Society of Petroleum Engineers, (2008).

[53] P. Pedenaud, P. Michaud, and C. Goulay. Oily-Water Treatment Schemes for Steam Generation in SAGD Heavy-Oil Developments. Society of Petroleum Engineers, (2005).

[54] W.F. Heins. Technical Advancements in SAGD Evaporative Produced Water Treatment. J Can Pet Technol, 48 (2009) 27.

[55] W.F. Heins. Technical advancements in SAGD evaporative produced water treatment. J Can Pet Technol, 48 (2009) 27.

[56] P. Pedenaud, F. Dang. A New Water Treatmetn Scheme for Thermal Development: The SIBE Process. Society of Petroleum Engineers, (2008).

[57] M.E. Welk, T.M. Nenoff, and F. Bonhomme. Defect-free zeolite thin film membranes for H_2 purification and CO_2 separation. Studies in Surface Science and Catalysis, 154 (2004) 690.

[58] M. Kanezashi, J. O'Brien, and Y.S. Lin. Template-free synthesis of MFI-type zeolite membranes: Permeation characteristics and thermal stability improvement of membrane structure. Journal of Membrane Science, 286 (2006) 213.

[59] F. Bonhomme, M.E. Welk, and T.M. Nenoff. CO_2 selectivity and lifetimes of high silica ZSM-5 membranes. Microporous and Mesoporous Materials, 66 (2003) 181.

[60] O. Korkuna, R. Leboda, J. Skubiszewska-Zie¸ba, T. Vrublevs'ka, V.M. Gun'ko, and J. Ryczkowski. Structural and physicochemical properties of natural zeolites: clinoptilolite and mordenite. Microporous and Mesoporous Materials, 87 (2006) 243.

[61] S. Khajavi, J.C. Jansen, and F. Kapteijn. Production of ultra pure water by desalination of seawater using a hydroxy sodalite membrane. J.Membr.Sci., 356 (2010) 52.

[62] F. David, V. Vokhmin, and G. Ionova. Water characteristics depend on the ionic environment. Thermodynamics and modelisation of the aquo ions. Journal of Molecular Liquids, 90 (2001) 45.

[63] M.Y. Kiriukhin, K.D. Collins. Dynamic hydration numbers for biologically important ions. Biophys.Chem., 99 (2002) 155.

[64] A.G. Volkov, S. Paula, and D.W. Deamer. Two mechanisms of permeation of small neutral molecules and hydrated ions across phospholipid bilayers. Bioelectrochem.Bioenerget., 42 (1997) 153.

[65] J. Zhou, X. Lu, Y. Wang, and J. Shi. Molecular dynamics study on ionic hydration. Fluid Phase Equilibrium, 194-197 (2002) 257.